MECHANICAL

TECHNOLOGY

INCORPORATED

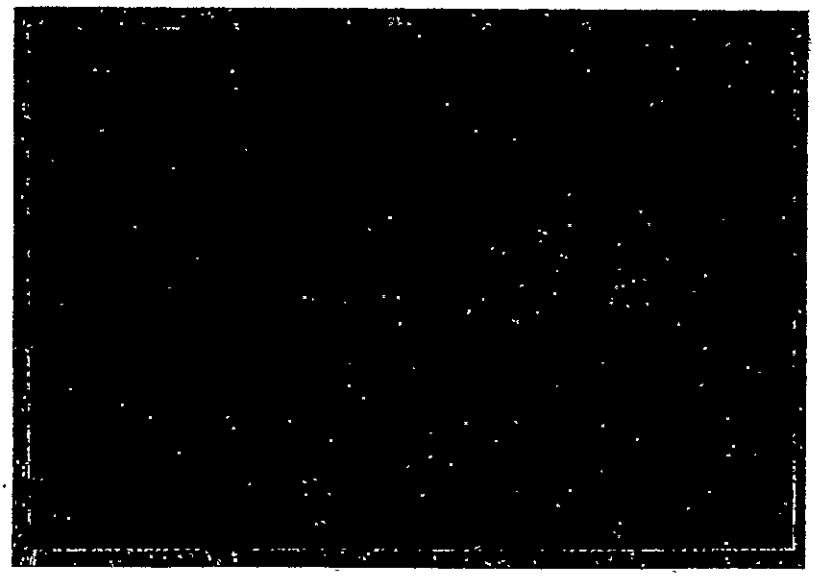

15

SOT.61980

NO. MTI-69TR38

DATE: November, 1969

TECHNICAL REPORT

STUDY OF HYDRODYNAMIC GYRO SQUEEZE-FILM BEARING

FINAL REPORT

by

T. Chiang
R. L. Smith

T. Chiang R. L. Smith

Author (s)

Approved

Approved

Prepared for

National Aeronautics and Space Administration
George C. Marshall Space Flight Center
Huntsville, Alabama

Prepared under

Contract: NAS 8-21169

MTI
MECHANICAL TECHNOLOGY INCORPORATED

968 ALBANY - SHAKER ROAD — LATHAM, NEW YORK — PHONE 785-0922

TABLE OF CONTENTS

MECHANICAL TECHNOLOGY INCORPORATED
968 Albany Shaker Road
Latham, New York 12110

MTI-69TR38

STUDY OF HYDRODYNAMIC GYRO SQUEEZE-FILM BEARING

FINAL REPORT

by

T. Chiang
R. L. Smith

November, 1969

I. INTRODUCTION

Mechanical Technology Incorporated has been under contract with George C. Marshall Space Flight Center, National Aeronautics and Space Administration to conduct a project, entitled "Study of Hydrodynamic Gyro Squeeze-Film Bearing". The primary objective of this project is to demonstrate the feasibility of employing squeeze film lubrication during starts and/or stops of the gyroscope wheel. A secondary objective is to gain some experience in the behaviors of hydrodynamic spiral-grooved spin-axis bearing.

An earlier phase of the contract (Phase I) dealt with the analytical aspects of the feasibility study [Ref. 1] and formulated the overall approach of the present phase, which concerns the experimental demonstration of the squeeze-film starts and stops.

The bread-board apparatus is built around existing parts of an experimental hydrodynamic gas bearing gyroscope wheel of the AB-5 size. The original "spool" type hydrodynamic gas bearing is replaced by a pair of opposed hemispherical bearings which are fixed on an out-board transducer fixture. The original motor drive is retained. The male bearings are spiral-grooved to enhance the hydrodynamic operation. A special conformal-masking technique and an electro-chemical etching procedure have been developed to put in the grooves on the male hemispherical bearings. The experimental study comprised mainly of the analysis of speed-time records of spin-ups and coast-downs with and without squeeze-film action.

This document contains all results and findings of the Phase II effort and is the final report of the contract.

II. MAJOR CONTRACT CHRONOLOGY

The first phase of the subject contract, a feasibility investigation and design study for a demonstration model, was performed in a timely and orderly manner. A report (MTI-67TR61) for this phase was issued. In the report, it was recommended that final design of the demonstration model be completed and a prototype be built.

Upon receiving NASA's approval of the Phase I report, MTI proceeded to complete the final design and initiated the procurement of the test apparatus and the spherical bearing units. At this stage of the program, progress was delayed on several occasions as a result of unforeseen difficulties in the fabrication of the bearing units as reported by the vendor, Athbro Engineering Corporation, Sturbridge, Mass. Such delay caused a serious impact on the program in that succeeding work could not proceed until all the components of the demonstration model were available.

In order to provide an understanding and appreciation of the events which contributed to the protracted performance period of the contract, a chronology of principal milestone events is presented below.

Major Milestone	Date
Beginning of Contract	June 28, 1967
Submission of Phase I Report	September 6, 1967
Approval of Phase II Program by NASA	October, 1967
Procurement of Test Apparatus	November, 1967
Procurement of Bearing Units (1)	March 14, 1968
Request for Time Extension (2)	September 9, 1968
Successful Etching of Grooves	March, 1969
Request for Additional Funds for Photo-etching of Grooves (3)	April 7, 1969
Commencement of Experiment	May, 1969
Issue of Final Report	November, 1969

Remarks for the Table

(1) MTI was informed by NASA, that the procurement of bearing units, originally to have been done by NASA, was to be performed by MTI. Athbro Corporation at Sturbridge, Mass., appeared to have a unique qualification in manufacturing the bearing units; they had the lapping equipment, the technical know-how and the gauge to measure spherical radius within the microinch range. This was essential because the tolerance of the bearing units was 5 microinches. Furthermore, Athbro Corporation has successfully provided bearing blanks (bearings without the grooves) of the same tolerance to MIT Instrumentation Laboratory. MIT has a grooving machine which can put spiral grooves on convex spherical surfaces with either a half inch or 0.656 inch diameter.

Based on the above, MTI issued a purchase order to Athbro Corporation on March 14, 1968 for the procurement of 5 male bearings and 4 female bearings. The delivery date agreed upon was June 13, 1968. Both Athbro Corporation and MTI had a tentative understanding from MIT Instrumentation Laboratory that Athbro Corporation could use MIT's grooving machine for this purpose, without interfering with MIT's own manufacturing schedule.

(2) Some delay in ordering the materials for the bearing units was encountered at Athbro, which caused a loss of time in meeting the delivery date. Then, near the completion of the final lapping, their gauges for measuring the spherical radius did not perform satisfactorily; they gave a floating reading of $\pm$ 30 microinches. With the assistance of Mr. Ken Taylor of MIT Instrumentation Laboratory and the gauge manufacturer, Athbro Corporation has worked very diligently and finally made the gauges function properly. A considerable amount of time was lost because of the malfunction of the gauges.

(3) When Athbro Corporation delivered the bearing blank, MIT was experiencing an extremely heavy load on their production schedule of grooved

spherical bearing, so that Athbro could not use their grooving machine. The situation persisted for more then two months and no relief was in sight.

MTI then proposed to photo-etch spiral grooves on male spherical bearings using a conformal masking technique. The photo-etching of spiral grooves on convex spherical surfaces was a success. The fund spent on photo-etching was not planned in the original contract. We therefore requested additional funds for photo-etching of grooves.

III. SQUEEZE-FILM TRANSDUCER DESIGN

An out-board construction is selected for the squeeze-film transducer. This provides ample room for locating the piezo-electric drive elements, the possibility of acoustic isolation between the relatively massive motor winding and the transducer, and permits adjustment of bearing gap after assembly.

A preliminary concept of the transducer, which originally appeared as a sketch in RFQ 1-7-40-79211, is shown in Fig. 1. It is seen that the gyro wheel is supported by two pairs of spherical bearings. The two male bearings are mounted on two flexures driven by a piezoceramic bar. The function of the flexures is to amplify the oscillatory motion of the piezo-electric bar and thus provide ample squeeze motion for squeeze-film bearing operation. The piezo-electric bar should be pre-stressed by, for example, tie bolts, so that the transmission of oscillatory motion from the piezo-electric bar to the flexures can be effectively achieved.

While this basic concept is generally retained, several refinements are introduced in the final design. They are enumerated as follows:

i. The length of the piezo-electric bar in this structure design is quite large. Therefore, the dimensional stability of the piezo-electric material may considerably affect the bearing clearance and thus impair the bearing performance. Shrink-fitted piezo-electric tubes operated either in thickness expansion mode (Fig. 2) or in thickness shear mode (Fig. 3) have been demonstrated to be feasible for the present application.

ii. Means will be provided in making both coarse and fine adjustments for the bearing clearance.

The final design of the demonstration model of hydrodynamic gyro squeeze-film bearing is shown in Fig. 4. Its features will be explained in detail in the subsequent sections.

In a gaseous squeeze-film bearing one of the bearing surfaces oscillates at a high frequency. This high frequency squeeze motion will generate a pressure in the film higher than the ambient and thus create load carrying capacity. There are two essential requirements for a squeeze-film bearing to be effective, namely, the squeeze frequency must be high and the normal component of the squeeze amplitude must be comparable to the mean gap. Since the squeeze amplitude one can obtain is limited, the latter requirement can only be met by specifying a small bearing gap.

The transducer has the dual function of supporting the non-rotating (male) element of the bearing and supplying a high frequency squeeze motion. The very small bearing clearance, of the order of 100 microinches, requires that the transducer structure be dimensionally stable to avoid changes in film thickness. A minimal of differential thermal expansion is therefore desirable and a method of making fine adjustments to the bearing clearance after assembly of the structure is essential.

Previous experience in transducer design for squeeze-film bearing application indicates that piezo-electric crystal is most suitable for the driving element because of its low power dissipation, low voltage, and light weight.

Mechanical joints in the structure must be held to a minimum because each joint dissipates a considerable amount of power in high frequency operation. Also, joints must be tightly clamped or heavily preloaded to minimize power dissipation. A final and important feature of the transducer is that it should be designed to operate with the motor stator and rotor of the existing experimental gyro as supplied by the Astrionics Laboratory.

The foregoing statements were reduced to the following set of criteria which governed the design of the bearing mount structure:

- The structure must amplify crystal motion either through geometry or through operation at a resonant frequency.

- Joints in the structure must be minimum in number and heavily preloaded.

- The structure must have a low coefficient of thermal expansion at least in the direction parallel to the bearing axis, since the wheel of the experimental gyro is made of alumina.

- A means of making fine adjustments in the bearing clearance after assembly must be provided.

- The structure should permit use of the motor stator and rotor of the existing experimental gyro.

These criteria are satisfied by the structural design presented below. The experimental evaluation of piezo-electric crystals driven in various modes is discussed in the next section.

A. Crystal Evaluation - Selection of Driving Mode

The criteria which evolved to govern the crystal selection were the following:

- The driving mode should offer efficient conversion of electrical energy to mechanical energy.

- Required energy input should be less than ten watts.

- A simple shape (circular, cylinder, or rectangular slab) is desirable to facilitate fabrication and mounting.

Since the driving mode of the crystal will ultimately determine the configuration of the support structure, data on various types of crystals were gathered. Two modes of piezo-electric crystal operation are particularly attractive from considerations of efficiency, reliability of system, accessibility of connections, and maximum amplitude of motion with minimum voltage.

The thickness expansion mode of crystal operation offers a d constant (meters/volt) of 285×10^{-12}. The coupling coefficient (K constant, see Ref. 9) for this

mode is .70 where $(K)^2$ is proportional to:

$$\frac{\text{Energy (Mechanical Out)}}{\text{Energy (Electrical In)}}$$

An experimental design was constructed (see Fig. 2) using a crystal tube 5/8 O.D. x 7/16 I.D. x 1/2 high. The crystal was split longitudinally to eliminate hoop stress and to equalize preload stress. It was placed on a metal rod and shrink-fitted into the metal structure using approximately a 2 mil interference (10,000 psi preload). Typical results show an amplitude of 160 microinches peak-to-peak at the ends and a frequency of approximately 20 KHZ at a power of 2.6 watts.

The other mode of interest is the thickness shear mode of operation. For this case the coupling coefficient is .71 and the d factor is 500×10^{-12}, a marked increase over the thickness mode. An experimental design was constructed (Fig. 3) using a crystal ring 1.250 O.D. x 1.00 I.D. x .500 high. This crystal was also slit longitudinally, slipped over the lateral rod and shrunk-fitted into both end plates with a 3.7 mil interference (approximately 11,000 psi preload). Typical results show an amplitude of 140 microinches peak-to-peak at 10 KHZ, with an input power of 2.1 watts.

The shear mode tests were repeated with the crystals clamped rather than shrunk in place. The clamp was fashioned from the end plates shown in Fig. 3. A saw cut was made along the vertical centerline from the bottom of each end plate into the hole where the crystal is mounted. A transverse hole was then drilled through the width of the lower end of the plate (below the crystal hole) to accept a through bolt. Tightening the nut on the bolt produced the desired clamping force on the crystal.

The clamped crystal performed satisfactorily though with somewhat lower amplitude than the shrunk-in crystal for a comparable power input. The reduced amplitude was probably due to the limited clamping force available from the through bolt.

The shear mode driver was selected for the demonstration model of the squeeze-film gyro bearing. It offered the following advantages over the thickness mode driver:

1. Ease of assembly. The bolted, clamped design facilitated assembly including coarse adjustment of the bearing clearance at assembly. The thickness mode driver was best assembled by shrinking. This is not a feasible method of assembly when using low-expansion alloys to minimize thermal expansion.

2. More effecient energy conversion. The shear mode has a higher d constant (strain per unit field) than the thickness mode.

3. Favorable orientation of preload force relative to pole direction. The shear mode crystal has the preload force oriented perpendicular to the poling direction. There is some evidence that this will tend to preserve the pole orientation. The thickness mode driver, on the other hand, has its preload force parallel to the poling direction which has a tendency to depole the crystal.

4. Redundant drivers. It was shown experimentally that the structure could be excited in the desired mode (end plates moving 180° out of phase) using only one of the driving crystals. Hence electrical failure of one driver does not mean complete failure of the gyro.

B. Structural Configuration

The structural configuration of the transducer is shown in Fig. 4 which is reproduced from MTI Drawing 198E02. A print of the drawing is also enclosed in the back cover. The configuration of Fig. 4 utilizes the shear mode of operation of the crystal whose feasibility has been demonstrated in a bench test as indicated in the last section.

The transducer structure consists of the non-rotating bearing elements, the

end plates which connect the bearings to the crystal drivers and preload the crystals and the bar connecting the two crystals in which the fine bearing adjustment is incorporated. The structure is symmetrical about the midplane of the gyro rotor so that bearing motions will be symmetric. The transducer is connected to ground (the bed plate) from the midpoint of the connecting bar. This also ensures symmetry of bearing motions.

A large through bolt is provided in each end plate to ensure that the necessary preload force can be applied to each driver without over stressing the bolt. The bolted clamp method of preloading the crystals is preferred to shrinking because it facilitates assembly and disassembly and permits coarse adjustment of the bearing gap.

The male spherical bearing, made of tungsten carbide, has a stem on the back. The stem is used to epoxy the bearing onto the end plate.

The female spherical bearing is epoxied to the gyro utilizing a spigot fit which tends to tighten as the rotor comes up to speed. The rotor supplied by NASA has been machined slightly so that it can accommodate the female bearings.

It is important to point out here that the bed plate and motor stator supporting structure are not part of the transducer design. They are simply a convenient stable base upon which to assemble and operate the motor, rotor and transducer. In addition to the support provided for the transducer, the bed plate supports the motor stator halves through the large angle brackets at either end. The bed plate and brackets are purposely made massive to minimize unwanted structural resonances and elastic distortion.

The fine adjustment feature of the design is best seen in Section C-C of the drawing. It consists of two bars which are connected at the ends to the crystal supporting hubs. The bars are bent slightly in mid span so that they are separated somewhat more in the center than at the ends. A threaded rod passes through a transverse clearance hole in the middle of each bar. A nut is positioned at the outside of each bar so that turning either or both nuts draws the

bars toward each other, straightening them in the process. The angle of the bend is chosen so that a very large reduction ratio is obtained between nut motion along the rod and axial separation of the bearing supporting end plates. The bars are spring loaded against the nut movement by a short section of thin walled tubing placed between the bars. A transverse clearance hole is provided in the tube to allow passage of the adjusting screw. As the nuts are tightened, the tubing is compressed along a diameter. The drawing shows a 3/8 inch diameter, .020 inch wall aluminum tube which has a spring constant of approximately 3650 pounds per inch.

The configuration shown on the drawing provides a 14 to 1 reduction of nut movement. Using a 56 pitch thread on the adjusting screw, this means that a five degree turn of a nut will change bearing clearance by 18 microinches. This is a reasonable measure of the sensitivity of adjustment. Total adjustment range of the device is defined as the movement which brings the bending stress in the bars to the yield point. If this is taken as 40,000 psi, the range of fine adjustment is 0.001 inch (or 1000 microinches). This appears ample. It is intended that the bearings be assembled initially with zero clearance. The fine adjustment will then be operated to provide clearance of the order of 100 microinches per bearing or 200 microinches total. Probes shown in Fig. 4 are for the purpose of measuring the clearance. The fixtures for the Fotonic Sensors are in a bench-test form, and are therefore not shown in the drawing.

The bolted clamp joint between end plate, crystal and connecting bar provides a means of coarse adjustment at assembly. One end plate will be clamped tightly over the crystal at one end of the connecting bar. The other will be slipped loosely over the other crystal while the rotor is inserted between bearings and the bearings are aligned. The bearings may then be held tightly together while the clamping bolt is tightened on the loose crystal. This should allow initial assembly with zero bearing clearance. This point will be discussed further in Section V.

IV. BEARING DESIGN STUDIES AND CALCULATIONS

The hemi-spherical geometry is chosen to minimize precision requirements in the transducer-bearing assembly since this configuration is insensitive to an end-to-end misalignment.

The plain-surface hydrodynamic journal bearing, whether cylindrical, conical, or spherical, is vulnerable to whirl-instability. This problem is particularly important in the case of gyro application since it can experience the radially unloaded condition where it is inherently unstable[Refs. 2, 3]. To overcome this limitation, shallow spiral-grooving of one of the bearing surfaces has proven to be effective [Ref. 7]. An analysis of spiral-grooved spherical bearings is given in Ref. 4, which indicated the advantages of spiral-grooving from the standpoints of stiffness, load, as well as stability. Although similar characteristics can be obtained by grooving either the male or the female surface, fabrication consideration was biased in favor of the former in the present case. Some sacrifice in squeeze-film load capacity and stiffness is caused by the presence of the spiral-grooves. This is because the grooves have reduced the effective squeeze-film bearing surfaces as will be explained in more detail later.

Since the bearing surfaces may come to solid sliding contact during the gyro start-up or coast-down without the help of the squeeze-film bearings, the bearing materials should be chosen to have low static friction and good sliding compatibility. Based on our past experience with bearing materials research [Ref. 8], we choose

Cemented Tungsten Carbide
(General Electric Carboloy 44A) for male bearing

Cold-Pressed $A\ell_2O_3$
(Coors-AD-99) for female bearing

The above materials also have good dimensional stability and low coefficient of thermal expansion.

A. Hydrodynamic Bearing Design and Calculations

The spiral-grooved spherical bearing configuration is shown in Fig. 5. The groove geometry is defined by the groove angle β, widths ratio a_g/a_r, groove depth δ and the number of grooves. The angles ω_E and ω_M give the extent of the grooved region.

The analysis of self-acting spiral-grooved spherical bearings has been formulated in Ref. 4. A computer program, which was originally restricted to the "vented" design, has been modified to analyze an "unvented"design for comparison. Two cases will be studied:

i. $\omega_p = 10°$

ii. $\omega_p = 0°$

In each case, the computer program is used to obtain optimum groove geometry for maximum stiffnesses and equal axial stiffness and radial stiffness at 24,000 rpm. The results are summarized as follows:

i. Vented bearing with $\omega_p = 10°$

Input: $\omega_E = 90°$

$\omega_M = 50°$

$\beta = 148°$

$R = 0.3125$ in.

C = 0.0001 in.

$h_g/h_r = 1 + \delta/h_r = 2.65$

$a_g/a_r = 0.84$

Output:

Spin Axis RPM	24,000	12,000
Axial Stiffness, lb/in	7.52×10^4	3.68×10^4
Radial Stiffness, lb/in	7.42×10^4	4.43×10^4
Tangential Stiffness, lb/in	7.13×10^3	1.14×10^4
Critical Mass, lb	2.06	16.4
Critical Whirl Ratio	1.3	0.7

ii. Unvented Bearing ($\varphi_p = 0$)

Input:

$\varphi_E = 90°$

$\varphi_M = 45°$

$\beta = 150°$

R = 0.3125 in.

C = 0.0001 in.

$h_g/h_r = 1 + \delta/h_r = 2.44$

$a_g/a_r = 0.3$

Output:

Spin Axis RPM	24,000
Axial Stiffness, lb/in	7.91×10^4
Radial Stiffness, lb/in	7.63×10^4
Tangential Stiffness, lb/in	1.46×10^4
Critical Mass, lb	8.5
Critical Whirl Ratio	0.615

It is seen that the two designs have approximately the same stiffnesses at 24,000 rpm. The critical masses are 2.06 lb. and 8.5 lb. for the vented bearing and the unvented bearing respectively. Since the mass of the rotor is approximately 0.3 lb., both designs are expected to provide stable operation. We note, however, that the a_g/a_r ratio is 0.84 for the vented bearing and 0.3 for the unvented bearing. In making the spiral groove pattern, etching method will be used as described

in Appendix A. Any inaccuracy in the layout of the groove pattern or in making the mask would result in some deviation for the designed groove and ridge widths. If the designed a_g/a_r ratio is small (or large), then an inaccuracy in the groove or ridge dimension can considerably change the a_g/a_r ratio from the designed value. It is, therefore, desirable to have the a_g/a_r ratio close to unity. For this reason we choose the vented bearing design with $\varphi_p = 10°$.

Due to the static weight of the rotor (0.3 lb) the bearing will be displaced from the concentric position by approximately 4 microinches at 24,000 rpm and 8 microinches at 12,000 rpm. Since the rotor mass (0.3 lb) is below the critical mass (2.06 lb at 24,000 rpm, 16.4 at 12,000 rpm), the bearing will be stable under the operating conditions indicated above.

B. Squeeze-Film Bearing Calculations

In the last section we have obtained an optimum spiral groove geometry according to its hydrodynamic performance. This geometry will be used as input to calculate its squeeze-film bearing forces.

The spherical bearing surface consists of a smooth portion ($\varphi = 10°$ to $50°$) and a grooved portion ($\varphi = 50°$ to $90°$). Suppose that the transducer can yield a squeeze amplitude of 80 microinch peak-to-peak. Then, for a bearing radial clearance of 100 microinch, we have an excursion ratio of 0.4. Let η_z be the axial displacement ratio and η_z is positive when the gap is opening up from the concentric position (see Ref. 5).

In the grooved portion of the bearing surface, only the ridge region is effective for the squeeze-film bearing. Even the ridge region does not contribute significantly to the squeeze-film forces compared to the smooth (ungrooved) portion of the bearing surface. Typically, take $\eta_z = -0.6$, $\varepsilon = 0.4$, $\Omega = 10{,}000$ cycle/sec., $R = 0.32$ in., $L = 0.036$ in., $\varphi_p = 10°$, $\varphi_M = 50°$ and $\varphi_E = 90°$. Then the dimensionless axial forces are as follows:

Due to the smooth (ungrooved) portion, 0.522
Edge correction to the smooth portion, -0.003
Due to the ridge regions, 0.019
Edge correction to ridge regions, -0.005

Thus, the total dimensionless axial force is 0.533. We summarized the results of the squeeze-film calculations in the following table.

η_z	$\frac{F_z}{p_a \pi R^2}$	$\frac{F_r}{\eta_r p_a \pi R^2}$
-0.6	0.533	0.479
-0.4	0.185	0.114
-0.2	0.112	0.060
0	0.076	0.037
0.2	0.056	0.025
0.4	0.042	0.018
0.6	0.033	0.014

There are two spherical bearings in the system and we denote the line connecting the centers of bearing by CC as shown in Fig. 3. We can operate the squeeze-film bearing with the following alternatives: (i) CC horizontal with the load supported by F_r. (ii) CC vertical with the load supported by F_z. (iii) CC in an arbitrary direction with the load supported by both F_r and F_z.

(i) CC horizontal

Suppose that $\eta_z = 0$ and $\varepsilon = 0.4$. We read from the above table that $F_r = 0.037\ \eta_r p_a \pi R^2$. If we are willing to operate the bearing at a radial displacement ratio of $\eta_r = 0.7$, there should be a factor of 3 [Ref. 6] to take the non-linearity due to large η_r into account. Since there are two bearings, there should also be a factor of 2. Thus, the radial force is

$$F_r = 0.037 \times 0.7 \times 2 \times 3\ \pi R^2 p_a$$

$$= 0.155\ \pi R^2 p_a$$

(ii) CC vertical

Suppose that the lower bearing is at $\eta_z = -0.6$ and the upper bearing at $\eta_z = 0.6$. Then, we can read from the table that $F_z = 0.533\ \pi R^2 p_a$ for the lower bearing and $F_z = 0.033\ \pi R^2 p_a$ for the upper bearing. The net force is

$$F_z = (0.533 - 0.033)\ \pi R^2 p_a$$

$$= 0.5\ \pi R^2 p_a$$

Therefore, it is desirable to operate the squeeze-film bearing in the CC vertical direction. The load capacity is given by

$$F_z = 0.5\ \pi R^2 p_a = 0.5\ \pi\ (0.32)^2\ 14.7$$

$$= 2.36 \text{ lb.}$$

For heavily loaded bearing, it is learned from our past experience that there is a factor of 1/4 between the theoretical and measured load capacities. Thus, the actual load capacity is estimated at $F_z = 2.36/4 = 0.59$ lb. Since the rotor weight is approximately 0.3 lb., there is a safe factor of 2.

V. PROTOTYPE BEARING DESIGN, ASSEMBLY AND ADJUSTMENT

The bearings used for the gyro rotor are two pairs of spherical bearings. The male bearings are spiral-grooved; one with left-hand grooves, the other with right-hand grooves. They should be assembled in accordance with the direction of rotor rotation so that the pumping action of the grooves is toward the pole region of the bearings. The male bearing radius is $0.328000\ ^{+0.000000}_{-0.000005}$ in. and the female bearing radius is $0.328075\ ^{+0.000005}_{-0.000000}$ in. With the above manufacturing tolerances, the male bearings and the female bearings are interchangeable; the radial clearance is in the range of 75 to 85 microinches before pre-etching. Assume that the pre-etching process takes away no more than 10 microinches. Then, the final radial clearance is in the range of 75 to 95 microinches.

The two female spherical bearings made of cold-pressed aluminum oxide were first epoxied on the rotor. The rotor originally supplied by NASA has been machined slightly to accommodate the bearings. After the epoxy had dried up, a final touch-up lapping was done on the female bearing surfaces to remove the distortion which may have resulted from the epoxy process.

Next, the two male bearings were epoxied onto the end plates. We now preassembled the gap-adjustment flexure (part 9 in Fig. 4), the crystals, the end plates and the rotor. We first tightened the bolt on one end plate to fix the end plate with the crystal and one end of the gap-adjustment flexure. Then the other end plate was slipped to the other end of the gap-adjustment flexure with the crystal in place. It was found that tightening the bolt on this end plate would elastically deform the structure sufficiently such that the desired bearing gap can not be set by the adjustment screw which has a range of 0.001 inch as reported earlier. Therefore it is necessary to shim the bearing gap by 2 to 3 mils to compensate for the anticipated structure deformation before tightening the tie bolt in the second end plate. Normally, it takes three or four trials before we can get the bearing clearance in the desired range.

The close tolerance of the motor stator required the final adjustment in orientation to be made after the spacial orientation of the rotor was completed. Four one-mil metal shims were inserted between the rotor and the motor stator fixing

it relative to the rotor. The stator end plate (part number 2, Fig. 4) was then brought into position with shims and tightened thus securing the motor stator in the proper place. The shim stock between the stator and rotor were checked as tightening proceeded to insure that distortions, caused by bolting, did not lock the rotor and stator together.

The motor stator, the male spherical bearings and the rotor were ultrasonically cleaned in Freon prior to each assembly.

At this point the motor was checked and it was found that one motor stator would drive the rotor to synchronous. It was decided to make tests with only one rotor stator in place since this allowed bearing gap adjustments by loosening and re-tightening one bolt in the end plate opposite the assembled motor stator.

Figure 6 is a photograph of the test fixture and some peripheral apparatus as it appeared during testing in the clean room. Shown in Figure 7 is the gyro rotor mounted between flexures with one half of the motor stator in place.

VI. EXPERIMENTAL RESULTS

Instrumentation and Drives

The principal measurements made are amplitudes of the squeeze motions and the rotor speed. Fiber-optic probes (manufactured by the Instruments Division of MTI under the trade name "Fotonic Sensors"), which may be operated under either the displacement or the reflectivity mode, were used for both measurements.

Squeeze-film motions were measured by a pair of Fotonic Sensors operating in the displacement mode. The sensitivity of the probe was 7.2 microinch per millivolt and the signal-to-noise ratio gave a ten microinch resolution. A dual-beam oscilloscope was used to determine the phase relation between the two bearings which moved with 180° relative phase when the transducer was properly excited.

Half of the gyro wheel rim circumference was painted black and a Fotonic Sensor operating in the reflectivity mode looking at the wheel rim provided the required tachometry. Output of the optical was read on a Hewlett-Packard Model 500B frequency meter and also recorded on a Hewlett-Packard Model 7035B X-Y recorder with a time base attachment to generate the speed-time data. A typical plot of start-up data as it comes from the X-Y recorder is shown in Figure 8. Note the small oscillations superimposed on the slope of the generated line. These small oscillations are indicative of the electronics used and must be averaged to obtain true frequency of rotation versus time plots. Another example of these oscillations is shown in Figure 9 where a touch down of the gyro was recorded. All subsequent plots will be redrawn averaged curves from original X-Y recordings for the sake of clarity. A recording of start-up to synchronous and coast down is displayed in Figure 10. The rotor axis was horizontal with a bearing clearance of 110 microinches and no squeeze film was present during the run shown.

The motor was driven by a three phase inverter which was in turn driven by a regular power supply unit. The inverter was a three phase four hundred cycles

per second static electronic inverter produced by Gulton Industries Engineering Magnets Division. The excitation voltage of the unit was twenty-five volts.

The direct current power supply used to drive the inverter was a product of Gates Electronics. It was a single phase unit with a voltage output range from zero to thirty-two volts and a current drawing capacity of forty ampheres.

The lead zirconate-lead titanate ceramic piezo-electric flexing crystal was driven during gyro testing in the conventional manner. A sine-wave from a Hewlett-Packard model 200 CD signal generator was fed into an audio amplifier. The voltage output from the amplifier was stepped up by a transformer with a turns ratio of one to ten. The operating voltage applied to the crystal was between one hundred to two hundred volts. The frequency at which one drives the crystal could be varied over the full audio range with the set up used. There were five resonant frequencies of the structure tested which yield sufficient amplitude to exhibit squeeze film action. However, only the major resonance at 4800 cps was used during all test runs of the gyro. The maximum peak-to-peak motion realized was about 400 microinches.

The flexures were also driven in the feedback oscillation mode of operation. In this method one crystal is driven by the output transformer from the amplifier while the other crystal is fed back into the input of the amplifier. The resonance of this mode is still 4800 cps but the vibration has some deviation from a pure sine wave. This is probably due to insufficient preload in the tie bolts of the crystals. For this reason, the open loop mode, driving the piezo-electric tubes with manually adjusted audio signal generator, was employed in conducting subsequent experiments.

Setting of Bearing Gap

A preliminary assembly and adjustment would be made prior to setting the bearing gap. The presence of some bearing clearance was established when the wheel could be freely spun up by a stream from the shop air directed tangentially at its periphery.

When the amplitude of the squeeze motion exceeded the available bearing gap, the oscilloscope display of the squeeze motion immediately became hashy. This was used to indicate the axial bearing clearance.

Although the transducer was designed to provide a coarse and a fine adjustment for setting the bearing gap, the latter cannot be utilized without disturbing the critical relative position between the motor stator winding and the gyro wheel. Therefore, bearing gap resetting with the motor stator already in place was done by repositioning the flexure arm on the opposite side of the winding. It was found necessary to reset the gap after extended testing (about two hours). Apparently, high amplitude squeeze motions would over come the clamping force which fastened the flexure(s) to the piezo-electric crystal(s).

Operation of the Gyro Wheel

After the gap has been set according to above, with one half of the motor stator assembled in place, the gyro rotor was readily run up to the design speed of 24,000 rpm, with the gyro axis either vertical or horizontal. In both cases the operation of the spiral-grooved spherical bearings was very smooth and no whirl instability was observed.

Excitation of the squeeze-film motion had virtually no effect on the operation of the gyro wheel at high speeds where hydrodynamic effects would dominate the load and stiffness characteristics and bearing torque would be negligible in comparison with windage torque. Therefore, most of the investigations were concerned with lift-off and touch-down characteristics. These studies were made with the various combinations of total axial clearance (end-to-end) ranging from 110 to 180 micro-inches, spin-axis vertical and spin-axis horizontal, and with and without squeeze-film motion.

Results of Lift-Off Recordings

A start-up recording with and without squeeze film was taken with the gyro axis vertical and is shown in Figure 11. The total axial bearing clearance was 110

microinches. No significant differences in start-up acceleration were noted above a rotor rotational frequency of five cycles per second. With and without the squeeze-film it took 0.6 and 0.9 sec. respectively for the rotor to reach the speed of 5 cycles per second. This difference is still small, indicating that the materials chosen for the bearings indeed provide very low sliding friction. It should be mentioned that five percent variations in acceleration were observed for successive start-ups under identical conditions. As lift-off occurred rapidly (usually between the first two or three revolutions of the rotor) precise acceleration values below five cycles per second were diffifult to obtain. A rubbing start is apparent in Figure 11 without squeeze-film with a lower acceleration rate until approximately 3 cycles per second, then lift-off occurred as evidenced by a sharp rise of acceleration. Once lift-off was achieved, until much higher speed is reached, the acceleration became limited and remained constant for a relatively extended period. At the lift-off point, the acceleration torque roughly doubled. Therefore, roughly half of the motor torque was needed to overcome the start-up contact friction. With squeeze-film, the acceleration assumed the inertia limited value from the very beginning.

Lift-off characteristics are relatively insensitive to the axial bearing clearance and whether the spin axis is vertical or horizontal as shown in Figure 12, at 180 microinches total axial clearance and spin-axis vertical, and in Figure 13, at 150 microinches total axial clearance and spin-axis horizontal.

In conclusion, the differences observed in start-up with and without squeeze film are observable but insignificant when compared to the contrasts which appear in coast-down.

Results of Coast-Down Recordings

Since coast-down with and without squeeze film was almost identical above a rotor frequency of seventy-five cycles per second, the following expanded traces of touch-down were taken. A typical set of coast-down data is displayed in Figure 14. The axis orientation was horizontal and the total axial bearing clearance was 150 microinches. The coast-down curves reveal a striking contrast between data taken

with and without squeeze film action. Although the start-up curves and the coast-down curves are both affected by contact friction, the latter is more revealing. Obviously the reason is that during coast-down the motor power supply is cut off, so that the coast-down curves are more sensitive to the friction. From the coast-down curve without the squeeze film in Figure 14, it is seen that the deceleration becomes large at about 10 cycles/sec. due to a very thin gas film (5 $\sim$ 10 microinches perhaps) and the deceleration becomes even larger at lower rotor speed and hence less hydrodynamic bearing action. At approximately 4 cycles/sec., sliding contact occurs. This brings the rotor to a rather abrup stop. With the action of the squeeze-film, however, the coast-down curve is much more gradual when the rotor speed is low; this is because a healthy gas film is maintained by the squeeze-film action.

The coast-down curves shown in Figures 15 and 16 are with the rotor axis vertical and with a total axial bearing clearance of 110 and 180 microinches respectively. These two sets of coast-down curves show similar behavior as those in Figure 14.

Another feature common in Figures 14, 15 and 16 is that when the rotor speed is, say, in 20 to 50 cycles/sec. range, the rotor deceleration with the squeeze-film action is slightly larger then that without the squeeze-film. This is rather unexpected and considered, at first, as some experimental uncertainty. A closer examination of the situation reveals that in this speed range (20 to 50 cycles/sec) the hydrodynamic action is quite adequate and the squeeze film does not appreciably increase the film thickness. However, the squeeze motion which is much faster than the rotation speed, causes the bearing gap to oscillate periodically about its mean value. The fluid friction with squeeze-motion, being proportional to the reciprocal of the bearing gap, would have a temporal average higher than that corresponding to that without the squeeze-motion (average of the reciprocal > reciprocal of the average for positive periodic functions).

Only when the rotor speed decreases to a value which is so low that due to the hydrodynamic action alone can not maintain a gas film, the squeeze-film action then becomes important and favorable in maintaining the rotor speed.

VII. SUMMARY AND CONCLUSIONS

A prototype hydrodynamic gyro squeeze-film bearing has been designed, fabricated, assembled and tested. Spiral-grooved spherical gas bearings were used for the gyro rotor support. The spiral grooves on the male spherical bearing were etched using a new technique developed under this program. With one half of the motor stator assembled in place, the gyro rotor was successfully driven to its design speed of 24,000 rpm. The rotor was running smoothly up through 24,000 rpm and whirl instability was not observed.

The squeeze-film transducer was able to provide a squeeze amplitude up to 400 microinches peak-to-peak at a frequency of 4800 HZ. The squeeze-film bearing was demonstrated to be able to support the rotor weight without the hydrodynamic action.

The start-up and coast-down data of the gyro rotor were taken both with and without the squeeze-film action. It was observed that during both the start-up and coast-down the squeeze-film bearing help to maintain a gas film; the effect is more evident in the coast-down data. The existence of the gas film during starts and stops eliminates sliding damage and reduces criticality of surface material problems. Also, since the start-up friction accounted for about one-half of the available motor torque, the squeeze-film action also eases electrical design requirement of the spin motor. The fundamental feasibility and the conceptual validity of squeeze-film start-stop assist for the hydrodynamic gas lubricated spin axis bearing have been experimentally demonstrated.

ACKNOWLEDGMENT

The authors wish to acknowledge Dr. C.H.T. Pan for his technical guidance and consultation in all phases of this project. This report represents the work contributed by many MTI personnel. In particular, we wish to express our appreciation to G. Moross for his work in preliminary transducer experiment, to D. McLaughlin and Keith Streifert for the transducer structure design, and to M. Russell for photo-etching the spherical bearings.

We are indebted to Mr. K. Taylor of MIT Instrumentation Laboratory for providing consultation in the measurement and fabrication of the spherical bearings.

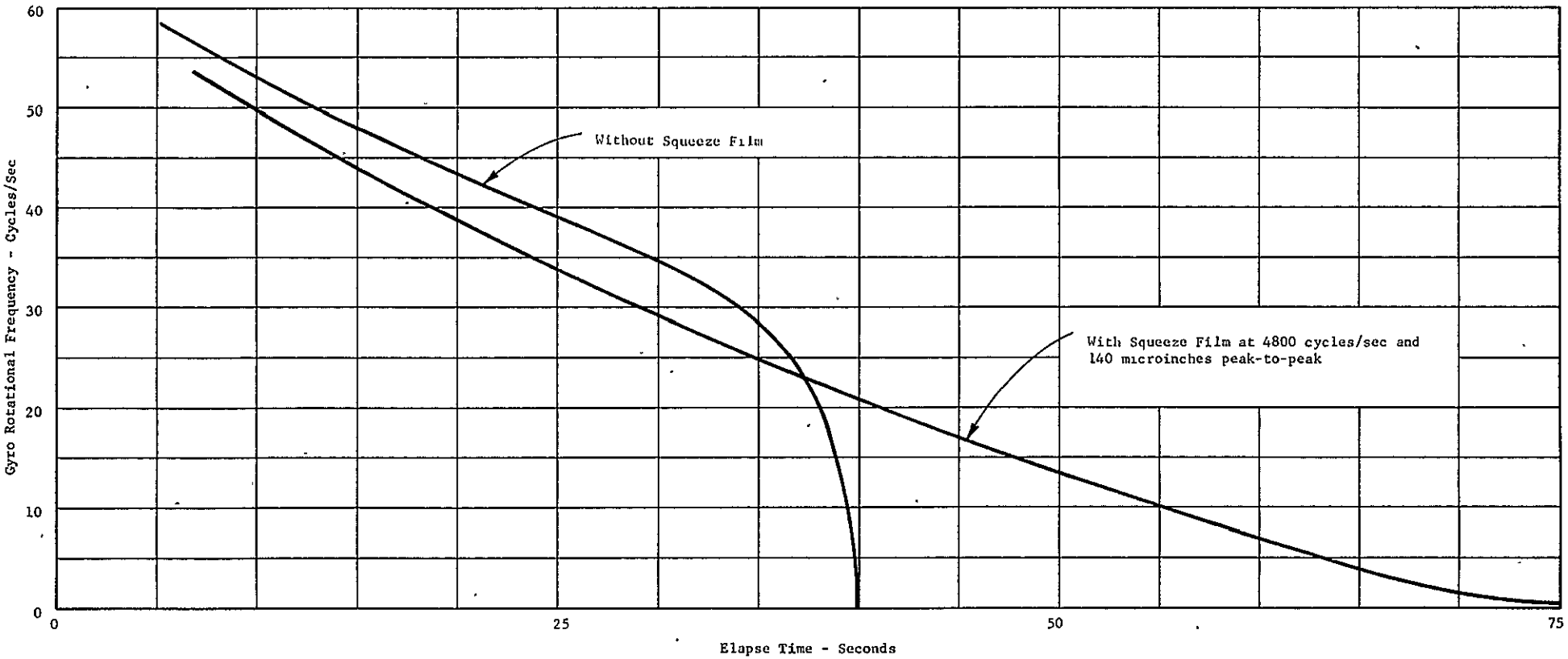

Fig. 16 Coast-Down Curves With and Without Squeeze Film With the Rotor Axis Vertical and a Total Axial Bearing Clearance of 180 Microinches

APPENDIX A

ETCHING OF SPIRAL GROOVES ON CONVEX SPHERICAL SURFACES

The etching of shallow grooves on developable surfaces, such as flat circular disk, cylindrical surface or conical surface, is not uncommon in obtaining grooved surfaces for bearing application. Various attempts were made in etching grooves on spherical surfaces. So far, these attempts were not successful; the main difficulty is that a spherical surface is not developable.

To deal with the situation, a conforming mask of almost exactly the same radius as the convex spherical surface is used. The mask is made opaque everywhere except for an area of one land (the area between two grooves) and in the area near the pole. This is for the configuration that the bearing has a grooved region near the equator and a seal region (ungrooved) near the pole. The male spherical bearing to be grooved is covered with a light sensitive photo-resist and inserted into the mask. Ultra-violet light from an electric arc lamp is shone through the "window" of the mask for a certain period of time. One then withdraws the male bearing from the mask, indexes to the next position and turns on the arc lamp again. The process is repeated until all the lands of the grooved region have been exposed and thus hardened. The bearing is now ready to be etched; only the grooves will be etched because the lands are protected by the hardened photo-resist.

The detailed preparations of the items mentioned above are described below in order.

(1) Preparation of the Spiral Groove Pattern

The spiral grooves on a spherical surface are defined to have a constant angle β with the latitude circles.

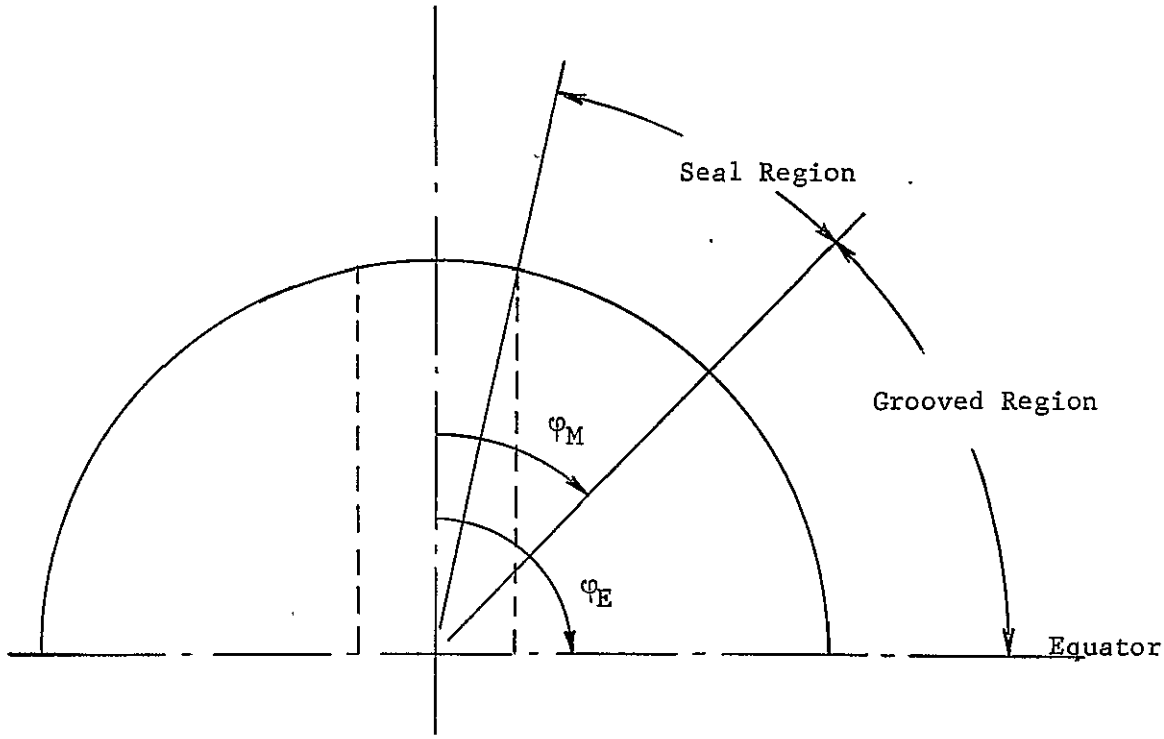

Let φ be the azimuthal angle and θ be the meridian angle. Let β' be the acute angle made by the groove center line and the latitude circles. Then, the differential equation for the groove is

$$\frac{-R\, d\varphi}{R \sin\varphi\, d\theta} = \tan\beta'$$

where R is the radius of the sphere, and $\beta' = 180° - \beta$.

The differential equation can be readily integrated to yield

$$\left[\ell n\ (\csc\varphi - \cot\varphi)\right]_{\varphi}^{\varphi_2} = -\tan\beta' \left[\theta\right]_{\theta}^{\theta_2}$$

If we choose $\varphi_2 = \varphi_E = 90°$ at which $\theta_2 = 0$, then we obtain an expression for the groove

$$\theta = - (\cot \beta') \ln (\csc \varphi - \cot \varphi)$$

Note that the sign of θ is not relevant because we have not defined the direction of θ yet. In fact, θ can go either way to give either left hand grooves or right hand grooves.

From the bearing design we have $\beta' = 32°$, $\varphi_M = 50°$ and $\varphi_E = 90°$, and we can easily carry out the computation and obtain the following table.

φ [deg]	θ [deg]
50	69.95
52	65.83
54	61.83
56	57.92
58	54.10
60	50.37
62	46.71
64	43.12
66	39.58
68	36.11
70	32.68
72	29.29
74	25.95
76	22.63
78	19.35
80	16.09
82	12.84
84	9.62
86	6.41
88	3.20
90	0.00

Now we can lay out one land strip on a spherical surface (knowing the number of grooves, the diameter and the width ratio). An ordinary globe of 12 inch diameter was used for the layout. A mylar film was laid over the globe and a piece of exactly (within the limits of craftsmanship) the same shape as the land strip was cut out. This piece was then photographically reduced to the correct size. The negative obtained provided a black background with a transparent section of the form of the land strip. The negative was used to photo-etch one land strip from a 0.001 inch brass shim stock. The resist used was Kodak KPR and the etch was Ferric Chloride.

(2) . Preparation of the Conforming Mask

The material chosen for the mask was General Electric's RTV-615. It has the desired physical properties of being compliant and yet stable and does not absorb an excessive amount of ultra violet light. It has a hardness of Shore A35.

The bearing is given a light coating of machinist marking dye. Three points along the edge of the land (the brass strip) are determined and laid out on the dye coating. The dye on the bearing is carefully removed except for small ring areas around the marked dots.

The brass land strip is then aligned with the dots under a microscope and cemented to the bearing surface (see Fig. 17). The cement used is a NITRATE base adhesive manufactured by Pactra Chemical Company, and is designated as clear - 65-1. It is essential that the brass pattern be in intimate contact with the bearing. Any raised edges would cause considerable trouble later. The bearing and its holding fixture are mounted on a stand which holds the bearing axis vertical in a pole downward position. A container for the mold (small plastic box) is placed around the bearing so it is square to the bearing axis. The RTV mold material is mixed and poured into the container so the level extends approximately one sixteenth of an inch above the equator of the bearing. The RTV is vacuum cured at 100°C for 3 hours. After being cured and cooled to room temperature the bearing is removed from the mold. The ragged edge and the edge of the impression should be removed and the mold wiped clean with a lint free cloth.

An opaque coating must then be applied to the spherical mold surface. This is done by first vapor deposit of aluminum followed by vapor deposit of gold.

The metallic coating must next be removed from the land impression. This is done by hand wiping, using sharpened wood dowling. This step should be done under a 40 X microscope with extreme care, because scratches in the coating cannot be repaired. If a scratch is made it will show up as un-etched area on the bearing, not once but the same number of times as there are grooves in the bearing. Therefore, if the coating is damaged, all of the deposited film must be removed and the

complete coating procedure repeated again. After removal of the coating from the land area, the mask is ready for use. One such mask with one right-hand land area is shown in the lower part of Fig. 18. Another mask with one left-hand land area was also prepared for making left-hand spiral-grooved bearings.

(3) Coating of Male Bearing (Spherical) Surface with Photo-Resist

The male spherical bearing made of Tungsten-Carbide was lapped to a very fine finish. In fact, the surface was so smooth that adhesion of the photo-resist on the surface became a problem, i.e. the photo-resist flaked away during etching resulting in zig-zag edges between grooves and lands. It is therefore necessary to "roughen" the bearing surface to insure adequate bonding of the resist. This was achieved by pre-etching the bearing surface lightly. The reduction in size due to pre-etching is very minute. Therefore, it is difficult to specify the pre-etching by the size reduction.

The correct amount of pre-etch was found to be when the surface loses its luster and assumes a grainy appearance viewed at approximately 5 times magnification. When the pre-etched surface is viewed under a 40 x microscope and the light is nearly parallel to the surface, the surface will be covered with bright "grains". It is believed that these bright areas are the original surface and the pre-etch is essentially intergranular.

The pre-etching procedure is as follows. Clean the bearing surface. Pre-etch for 30 seconds at 80 milliamps in 10% aqeous solution of oxalic acid. Rinse and wipe clean. The above procedure can be repeated 3 to 4 times to obtain the desired pre-etch. The pre-etched bearing is then cleaned with acetones followed by alcohol and dried in an oven at 100°C for 1/2 hour. After drying, the bearing should be cooled to room temperature then coated with photo resist. Immediately prior to use, the resist should be thinned 2:1 to produce a mixture of approximately 150 centi-stokes in viscosity. The bearing is submerged in the resist then quickly removed and put in the vertical (pole upward) position. The resist is allowed to air dry in darkness for a period of approximately 10 hours. After air drying and immediately prior to exposure the resist should be oven-dried at 110°C for 10 minutes.

(4) Photo-Etching

The bearing coated with photo-resist is mounted on the indexing head of a milling machine. The mask is clamped in a holder which is held in the spindle of the milling machine (Fig. 19). The indexing head is set to 0 degrees and the bearing is brought into position in the mold. The centering operation is unfortunately performed entirely "by eye". The bearing is brought up into the mold and centered in the horizontal planes so there is no noticeable deformation of the mold. The bearing is then moved in the vertical plane until slight deformation of the mold occurs. From the top of the land pattern upward to the pole is an area cleared of the metallic coating. This area is not recessed as is the land pattern. The bearing is lowered 20 or 30 mills and then raised while watching this cleared pole area. As the bearing comes in contact with the mold a change in color will be noted in the cleared area. As the bearing is further raised the coloration should move downward from the pole to the top edge of the recessed area. At this point, the correct height has been obtained. The bearing is then moved horizontally in a direction that will cause closer contact between the bearing and the mark at the land area. This motion is continued (approximately 5 to 10 mills) until contact is noted between the mask and bearing in the recessed area. At this point, the correct position for exposure has been reached.

The light source for exposure is supplied by an 8 amp carbon arc 9 inches away and 1" above the center of the bearing. Exposure time is 8 to 9 minutes for each land. The arc is turned on and the resist exposed for the correct period of time. After exposing the first land the bearing is lowered, indexed to the next position, and brought back to the same dial settings, for the next exposures. This process is repeated until all of the required lands have been exposed. The fully exposed bearing is then removed from the mask and soaked, with mild agitation, in KMER Developer for 3 to 4 minutes. The bearing is removed from the bath, immediately sprayed with KMER Developer, and air dried. If some areas require further image development, it should be done with the spray. During later work it was discovered that developing with straight KMER Thinner produced improved resolution. After the image has been satisfactorily developed, it should be baked at 135°C for one hour, then cooled to room temperature. After reaching room temperature the resist coating

may be "touched up" under the microscope. Excess resist or spots, caused by flaws in the mask, may be removed with a scraper. Areas where the resist coating is thin or missing may be painted with 2:1 KMER thinner mixture. If resist is painted on, it must be exposed prior to etching because the non-polymerized resist has very poor adhesive qualities. The bearing is now ready for etching.

The etching as well as the pre-etching is done electrolytically. A solution of 10% oxalic acid crystals in water is used. The rate of etching is controlled by the following factors: solution concentration, solution freshness, electrode size, electrode spacing, applied voltage, and time. The tungsten carbide male bearing is the anode and a hollow sphere with one inch radius was machined in a block of 304 stainless steel for the cathode (Fig. 20). The bearing is inserted into the cathode. A clearance of 1/16 inch at the pole region is set.

A very slow etch rate (80 milliamps for 12 minutes) was used for the first few test pieces. It was discovered later that the slow etch rate was apparently responsible for the under-etch at the groove-land boundaries. A few experiments with different current and time combination led us to choose a current of 3 amp and an etching time of 16 sec. For grooves 0.060 in. wide, 0.0002 in. deep, the under-etch is about 0.001 in.

The etching pot (suitable glass beaker) is filled with the oxalic acid mixture until the level has risen above the equator of the bearing (Fig. 21). There is a textolite spacer that is used to separate the bearing outer surface from the holding fixture. The liquid level should come half way up the spacer. If the electrolite comes in contact with the holding fixture, the etching process will be totally altered. The power supply is turned on and a current of 80 milliamps is set up. After operating at this low current setting for 10 to 20 seconds the current is quickly raised to 3 amps. The etch rate for 16 groove bearings at this high current setting is approximately 12.5 μ in/sec. It is recommended that when bearings are etched, they be rotated to help provide an even depth of etch.

After etching, the bearing is rinsed and dried. The bearing is then blasted with glass beads to remove any loose material or smut left by the etch. The resist is then stripped using KMER thinner. The bearing is now ready for cleaning and use (Fig. 22).

NOMENCLATURE

a_g, a_r	widths of groove and ridge (see Fig. 5)
C	mean clearance
e	excursion amplitude
F	force
h_g, h_r	film thickness in the grooved and ridge regions respectively
L	average width of ridge
M_c	critical mass
P_a	ambient pressure
R	bearing radius
β	groove angle
δ	groove depth
ϵ	excursion ratio = e/C
η_r, η_z	radial and axial displacement ratios
ϕ	azimuthal angle

Subscripts:

E	equator
P	pole
r	radial
z	axial

REFERENCES

1. T. Chiang, D. McLaughlin and C.H.T. Pan, "Study of Hydrodynamic Gyro Squeeze-Film Bearing, Phase I Feasibility Investigation", MTI-67TR61, 1967.

2. C.H.T. Pan, "Gas Lubricated Spherical Bearings", Journal of Basic Engineering, Trans. ASME, Series D, Vol. 85, 1963, pp. 311-323.

3. C.H.T. Pan and T. Chiang, "Dynamic Behavior of the Spherical Squeeze-Film Hybrid Bearing", Journal of Lubrication Technology, Trans ASME, Series F, Vol. 91, 1969, pp. 149-160.

4. S. B. Malanoski, "Gas-Lubricated Spiral-Grooved Spherical Bearing", MTI-64TR4, 1964.

5. T. Chiang, S. B. Malanoski and C.H.T. Pan, "Spherical Squeeze-Film Hybrid Bearing with Small Steady-State Radial Displacement", Journal of Lubrication Technology, Trans. ASME, Series F, Vol. 89, 1967, pp. 254-262.

6. S. B. Malanoski, and C.H.T. Pan, "The Solution of Special Squeeze Film Gas Bearing Problems by an Improved Numerical Technique", MTI-65TR26, February, 1966.

7. J. H. Vohr and C.H.T. Pan, "Gas-Lubricated Spin-Axis Bearings for Gyroscopes", MTI-68TR29, 1968.

8. S.F. Murray and M. B. Peterson,"The Selection and Evaluation of Materials and Lubrication Films for Gas-Lubricated Gyroscope Bearings", MTI-64TR1, 1964.

9. American Institute of Physics Handbook, Second Edition, p. 3-98, McGraw-Hill Book Co., 1963.

LIST OF FIGURES

LIST OF FIGURES (Continued)

Figure Number

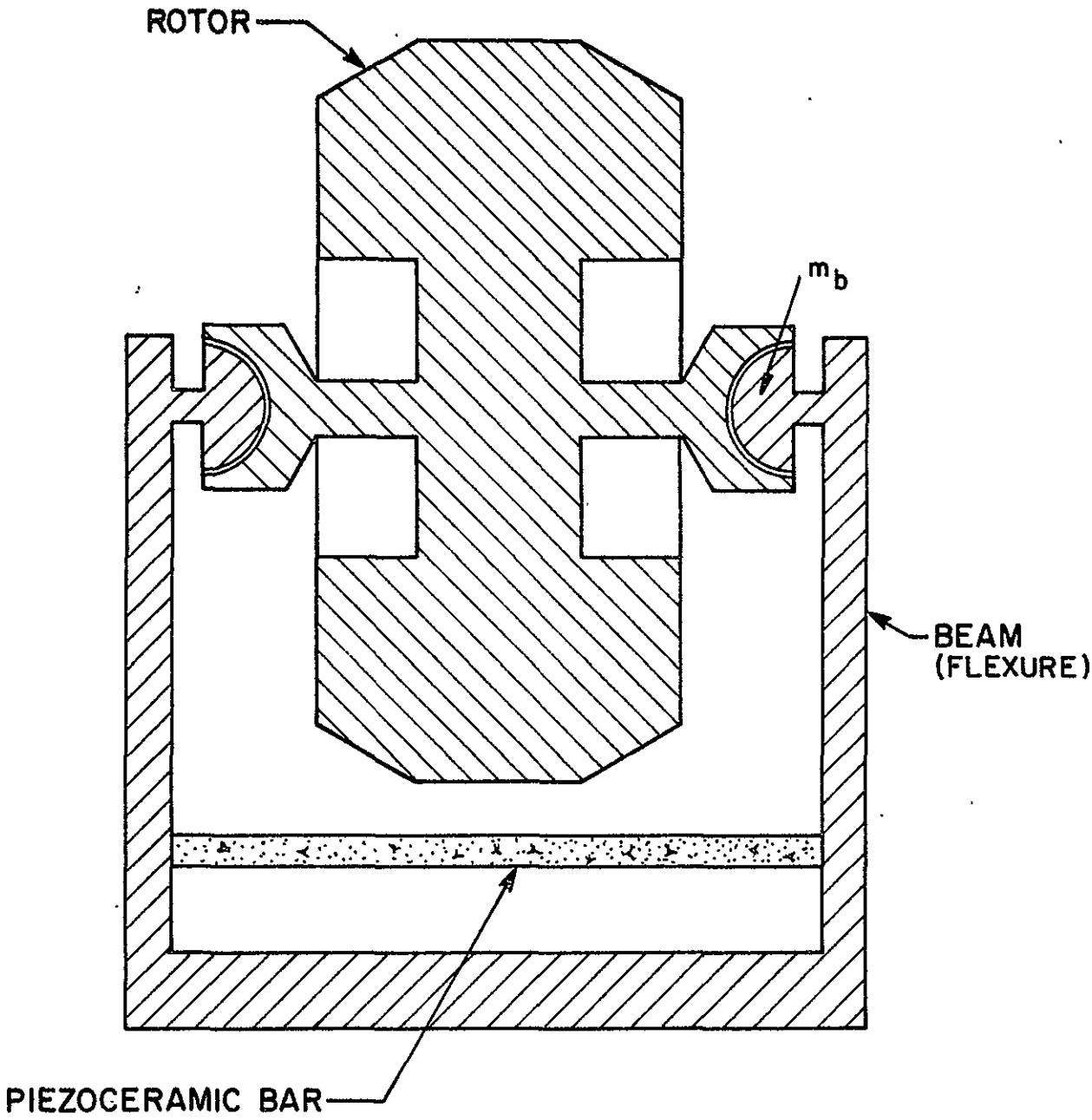

Fig. 1. Preliminary Structure Design for Hydrodynamic Gyro Squeeze-Film Bearing (Attacked Sketch in RFQ 1-7-40-79211)

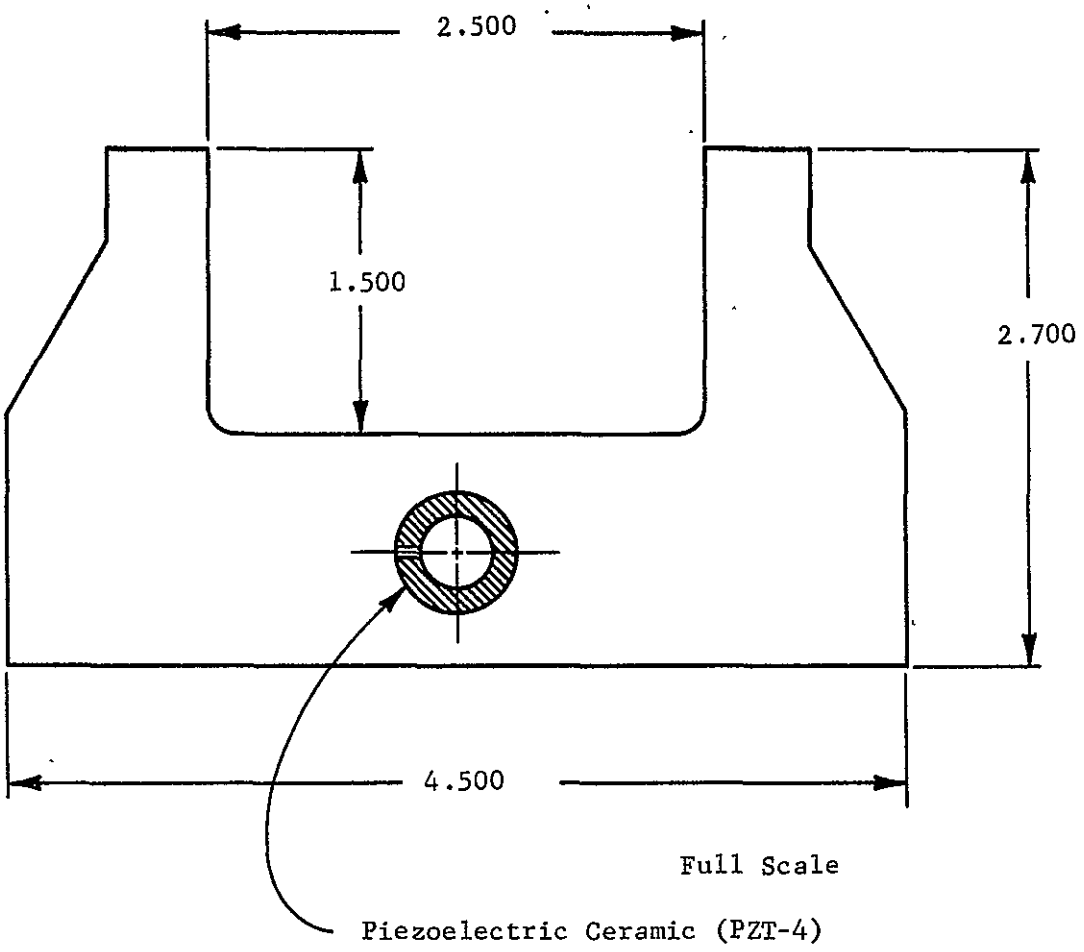

Fig. 2 Experimental Transducer - Shrink-Fitted Piezoelectric Ceramic Operated in the Thickness Expansion Mode

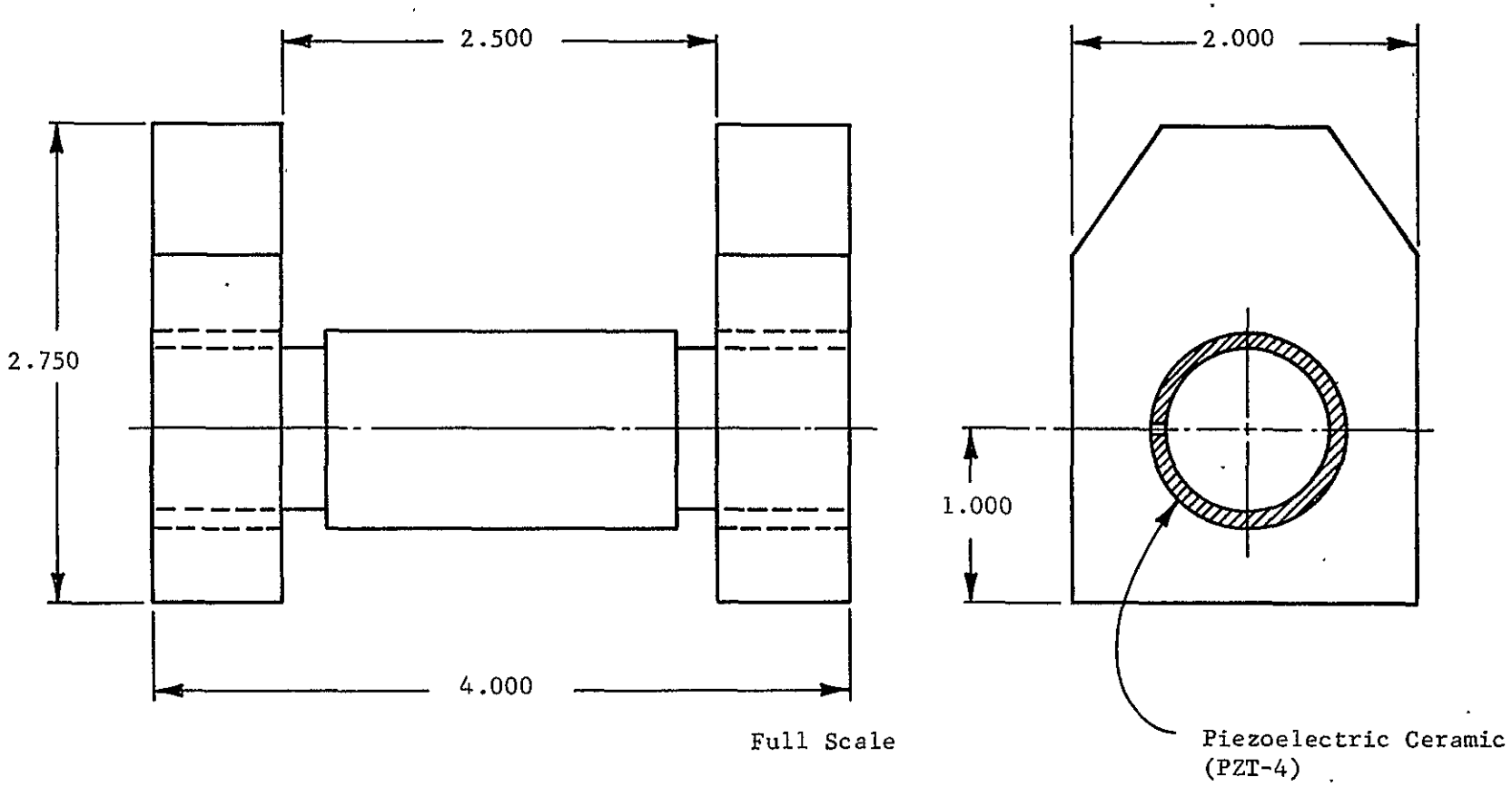

Fig. 3 Experimental Transducer - Shrink-Fitted Piezoelectric Ceramic Operated in the Thickness Shear Mode

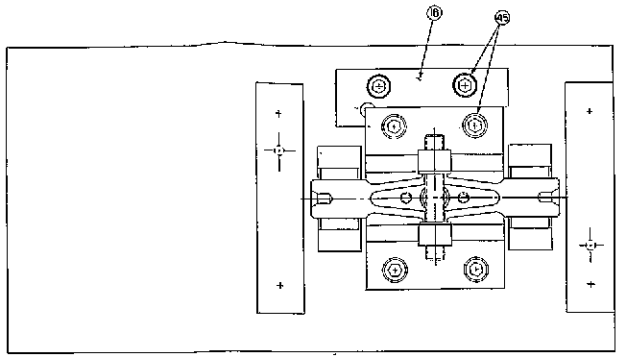

SECTION C-C

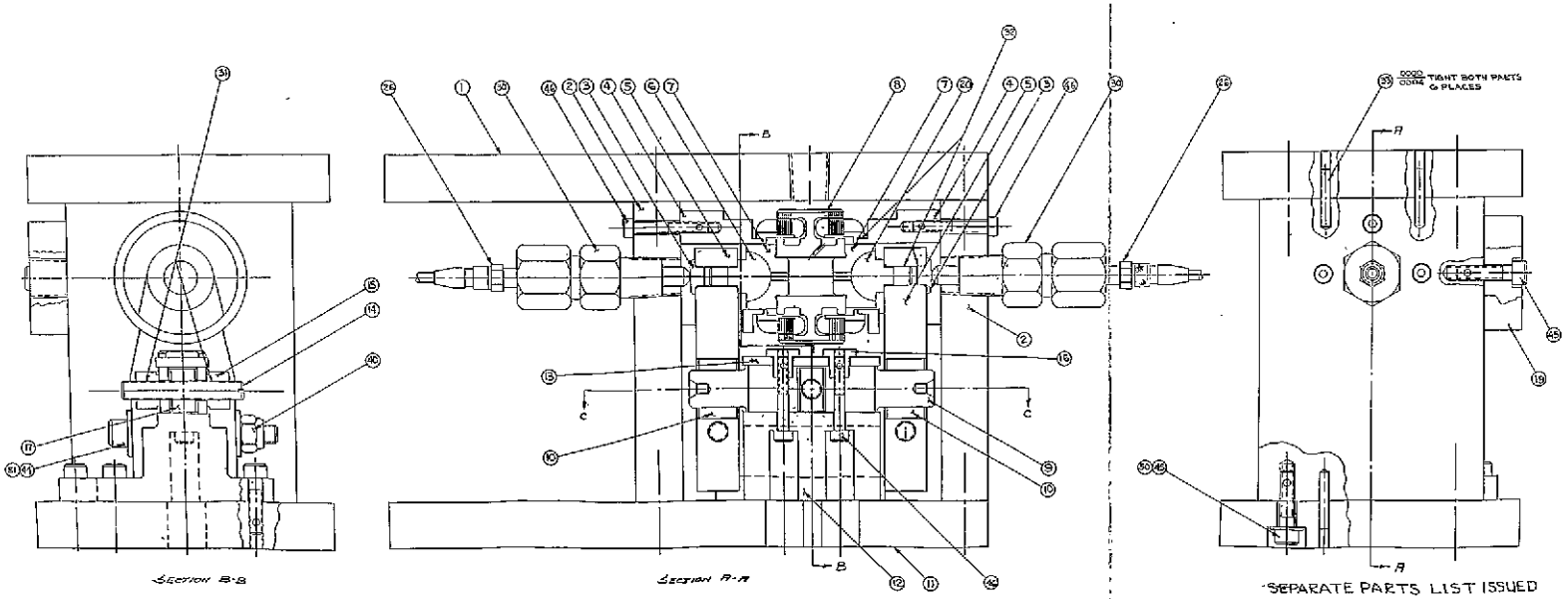

SECTION B-B

SECTION A-A

SEPARATE PARTS LIST ISSUED

FOLDOUT FRAME

Fig. 4 Demonstration Model - Hydrodynamic Gyro Squeeze-Film Bearing

FOLDOUT FRAME 2

ANL-7621

MECHANICAL TECHNOLOGY INCORPORATED

PL198E02
sheet 1 of 3

Title PARTS LIST FOR
ASSEMBLY DEMONSTRATION MODEL
HYDRODYNAMIC GYRO SQUEEZE-FILM BEARING

Quantity Per Group						Item No.	Part No.	Description
6	5	4	3	2	1			
					X		198E02 G1	ASSEMBLY
					1	1	198C15 P1	TOP PLATE
					2	2	198C10 P1	END PLATE
					2	3	198 B17 P1	BUTTON
					2	4	198 C11 P1	STATOR MOUNT
					2	5	198C08P1	END PLATE
					1	6	198 B04P1	JOURNAL SPHERICAL BEARING
					2	7	198 B03P1	BEARING SPHERICAL
					1	8	198B21P1	WINDING ASSEMBLY
								STATOR MODIFIED
					1	9	198C06P1	GAP ADJUSTMENT FLEXURE
					2	10	198B09P1	CRYSTAL
					1	11	198C16P1	BOTTOM PLATE
					1	12	198C12 P1	FLEXURE MOUNT
					1	13	198B18P1	FLEXURE PLATE
					1	14	198 B07P1	STUD
					2	15	198 B07P2	NUT
					2	16	198B19P1	NUT
					1	17	198B20P1	TUBE
					1	18	198B13P1	POSITIONING PLATE
					1	19	198C14 P1	SIDE PLATE
					1	20	198B04P2	JOURNAL SPHERICAL BEARING

Approved H. JONES 3/5/68
Checked RS 3-4-68
Drawn H. Bartnicki 29 JAN '68

Rev. No.

PL198E02
sheet 1 of 3

MECHANICAL TECHNOLOGY INCORPORATED

PL198E02
sheet 2 of 3

Title

ASSEMBLY DEMONSTRATION MODEL
HYDRODYNAMIC GYRO SQUEEZE FILM BEARING

Quantity Per Group						Item No.	Part No.	Description
6	5	4	3	2	1			
					2	26		CAPACITANCE PROBE WITH
								LEAD .250 O.D. X 2.5 LONG
								3 ELEMENT .001 RANGE
								TAPERED END - STANDARD
					2	30	PG2-250-A-N	PACKING GLAND
								CONAX CORP OR EQUIV.
					AR	31		LOCKTITE SEALANT
								TYPE HV
					AR	32		EPOXY - SCOTCHWELD #2214
					6	33		DOWEL PIN - .125 DIA. X .750
								LONG - STEEL.

Approved H JONES 3/5/68
Checked RS. 3-4-68
Drawn J Bartnicki 29 JAN. '68

Rev. No.

PL198E02
sheet 2 of 3

MTI-7657

MTI
MECHANICAL TECHNOLOGY INCORPORATED

PL198E02
sheet 3 of 3

Title PARTS LIST FOR
ASSEMBLY DEMONSTRATION MODEL
HYDRODYNAMIC GYRO SQUEEZE FILM BEARING

Quantity Per Group						Item No.	Part No.	Description
6	5	4	3	2	1			
					2	40	CAT.#2INE-048	NUT- ELASTIC STOP NUT
								CORP OR EQUIV.
					2	44		HEX. SOCKET HD. CAP SCREW
								1/4-28 x 2.00 LONG STEEL
					16	45		HEX. SOCKET HEAD CAP SCREW
								(NYLOK) #10-32 X .75 LONG STL.
					8	46		HEX. SOCKET HD. CAP SCREW (NYLOK)
								#6-32 X 1.00 LONG STEEL
					8	50		WASHER (FOR #10 SCREW)
								7/16 O.D. x 1/32 THICK L.C. STEEL
					4	51		WASHER (FOR 1/4 DIA. SCREW)
								5/8 O.D. x 1/16 THICK L.C. STEEL

Approved H. Jones 3/5/68
Checked R.S. 3-4-68
Drawn T. Bartnicki 29 JAN. '68

Rev. No.

PL198E02
sheet 3 of 3

MTI-7658

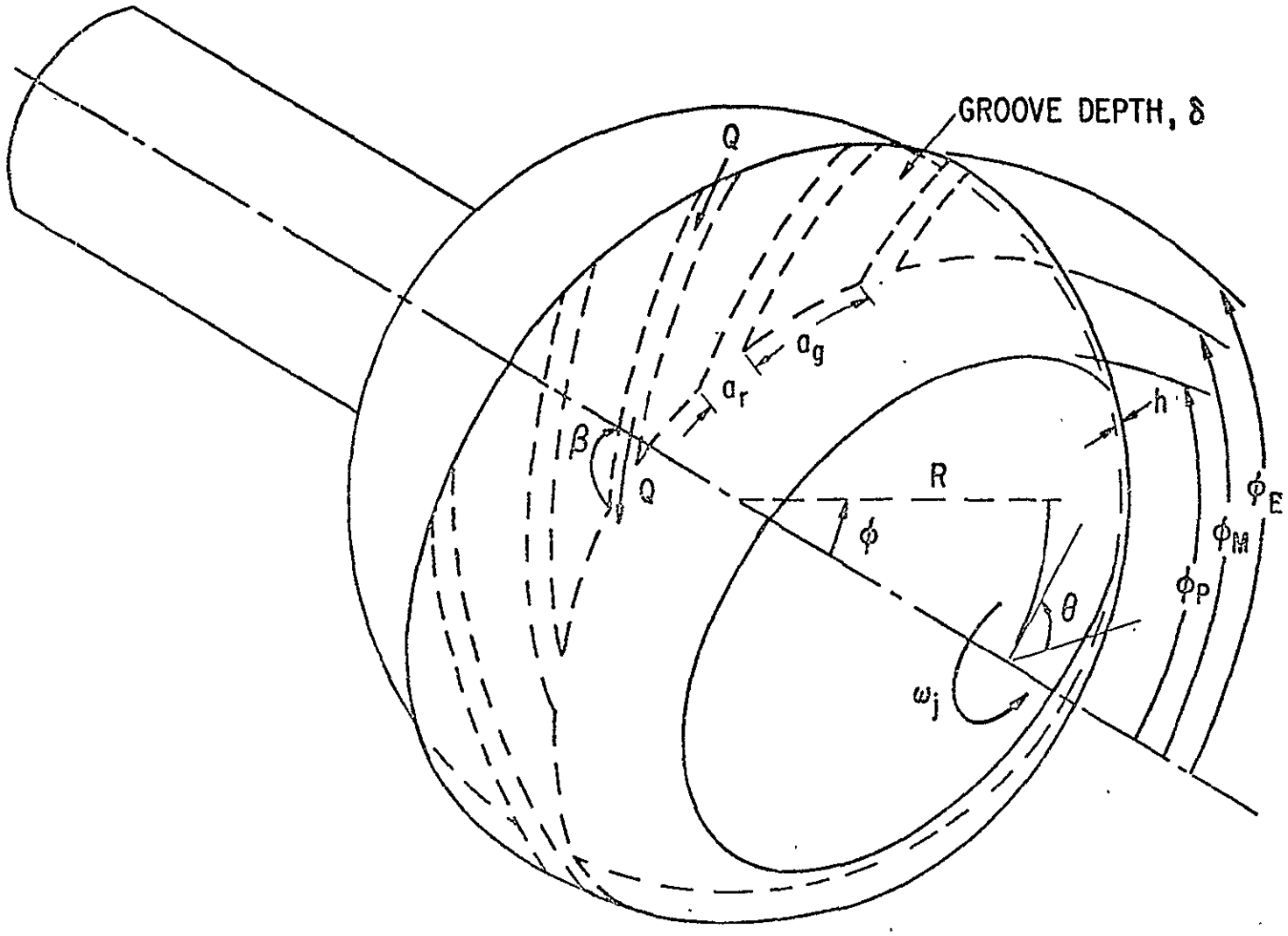

Fig. 5 Schematic of a Spiral-Grooved Spherical Bearing

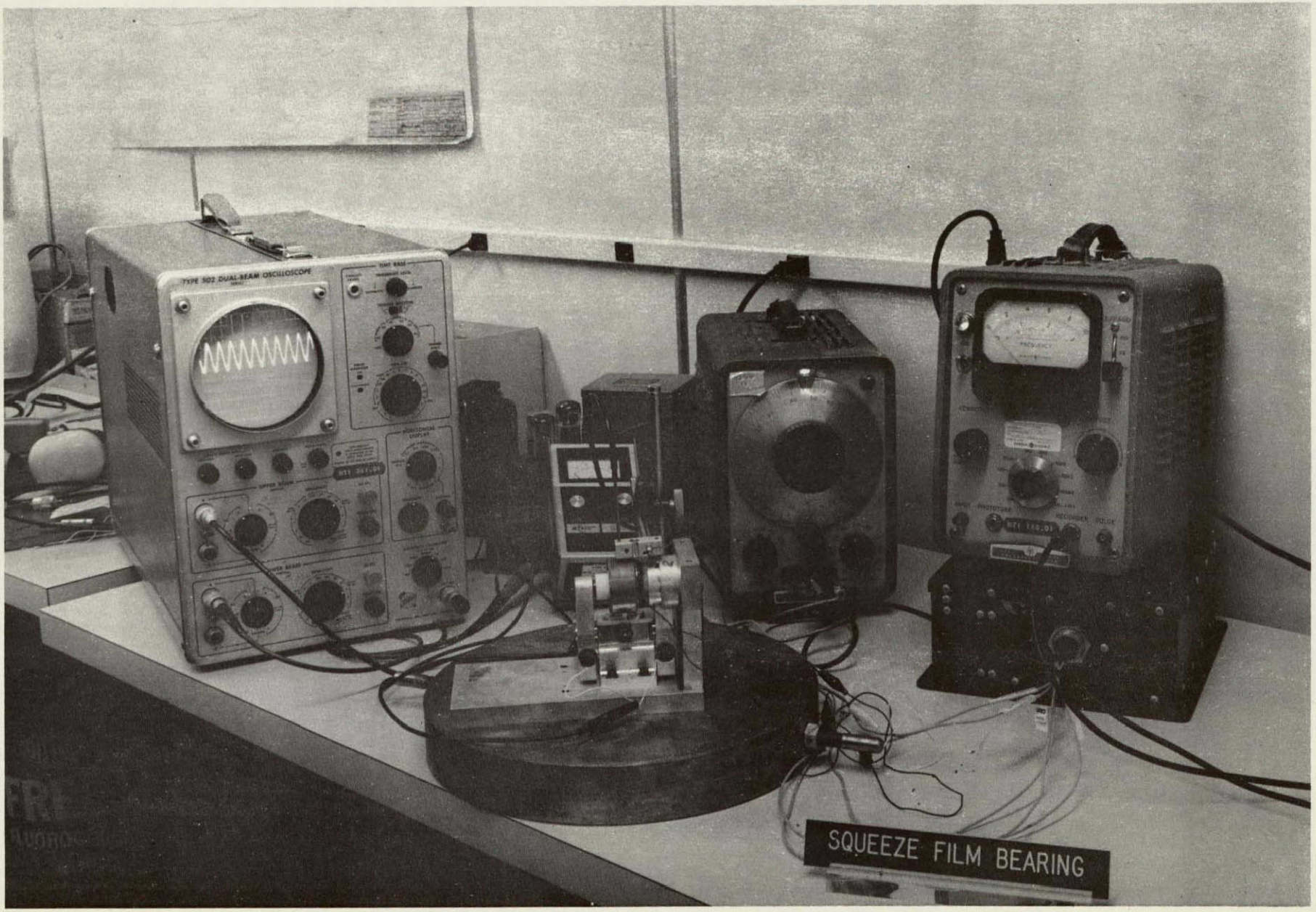

Fig. 6 Hybrid Squeeze Film Bearing Test Facility

MTI-7652

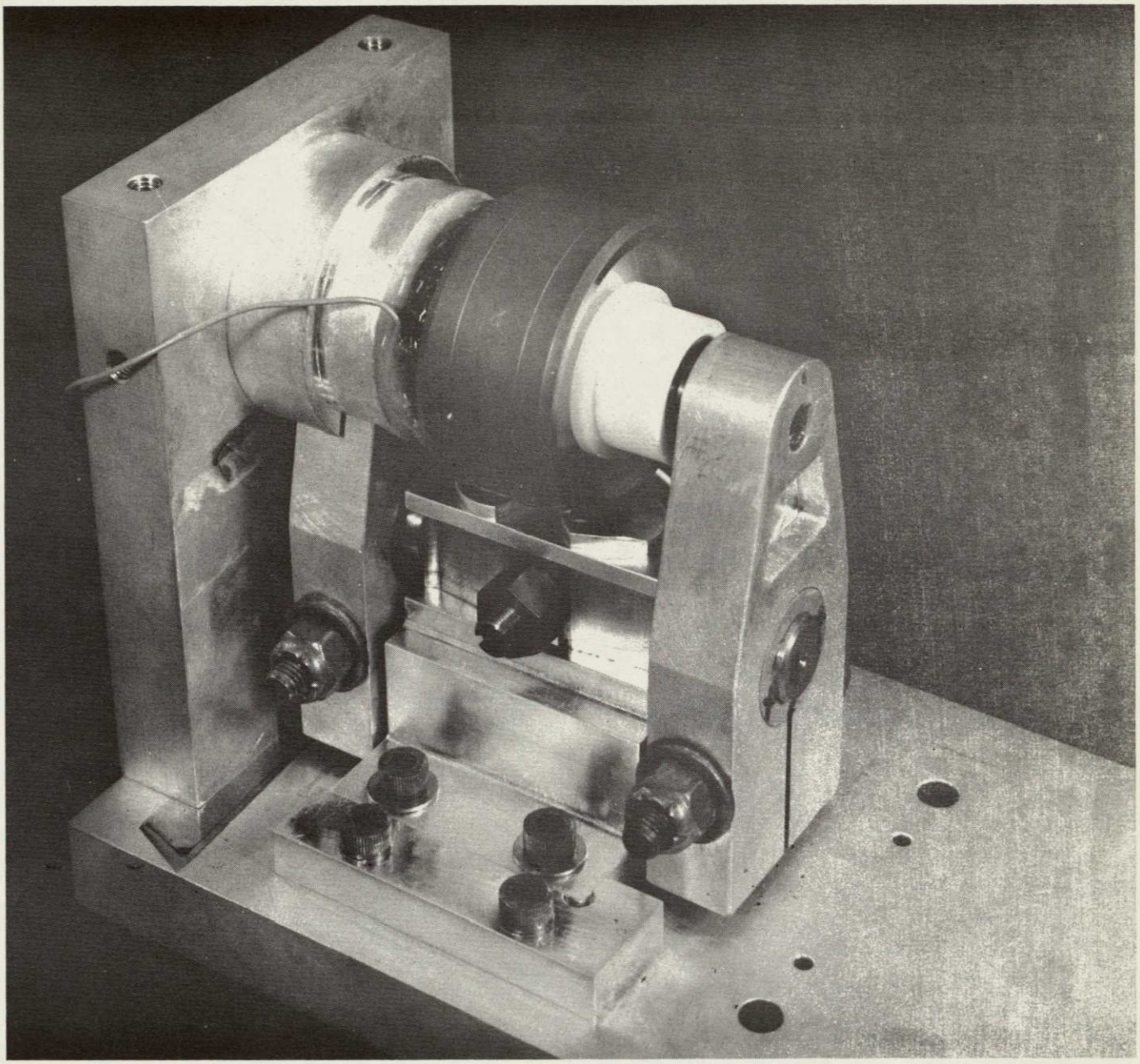

Fig. 7 The Gyro Rotor Mounted Between Flexures with One Motor Stator in Place

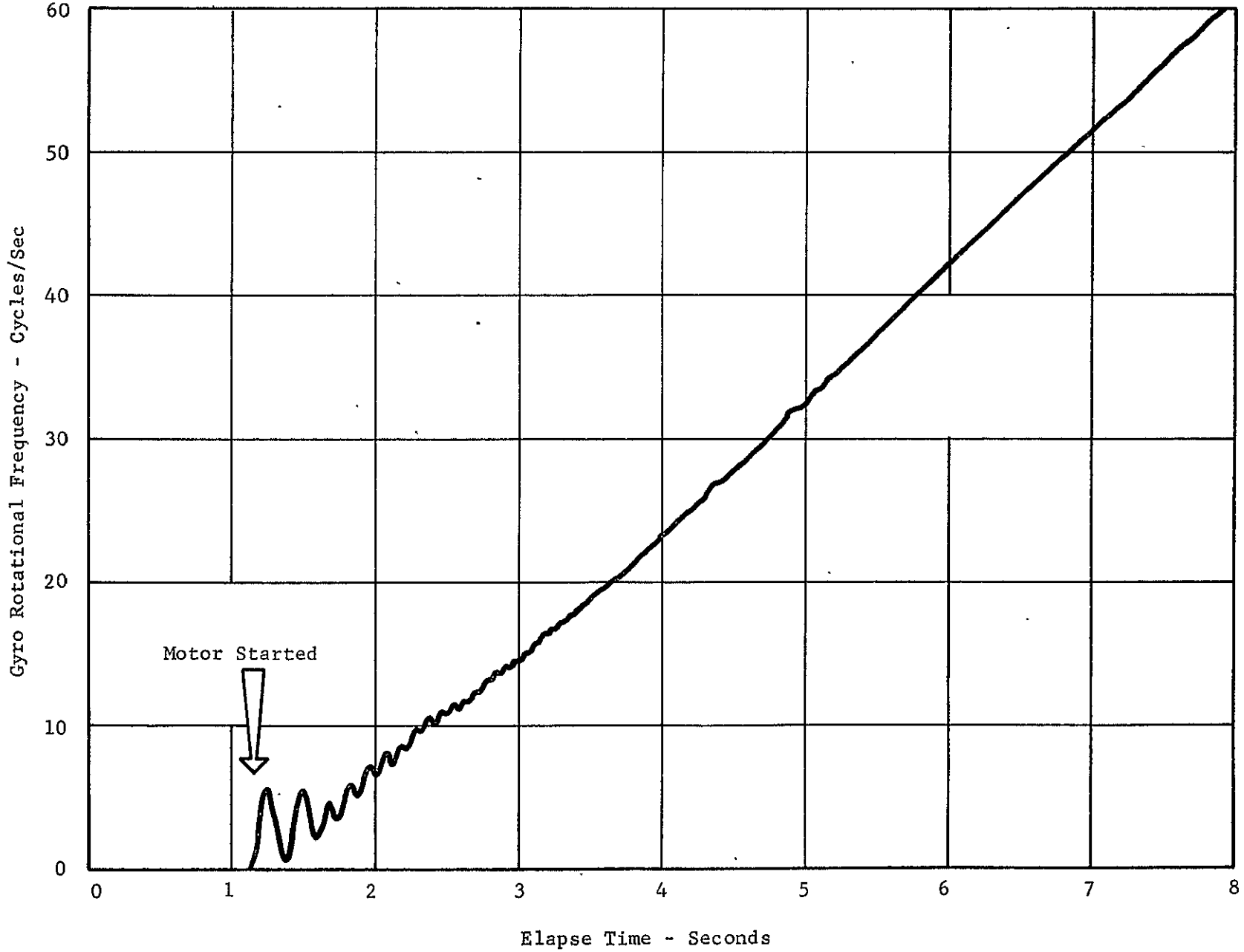

Fig. 8 A Typical Plot of Start-Up Data from the X-Y Recorder

MTI-7661

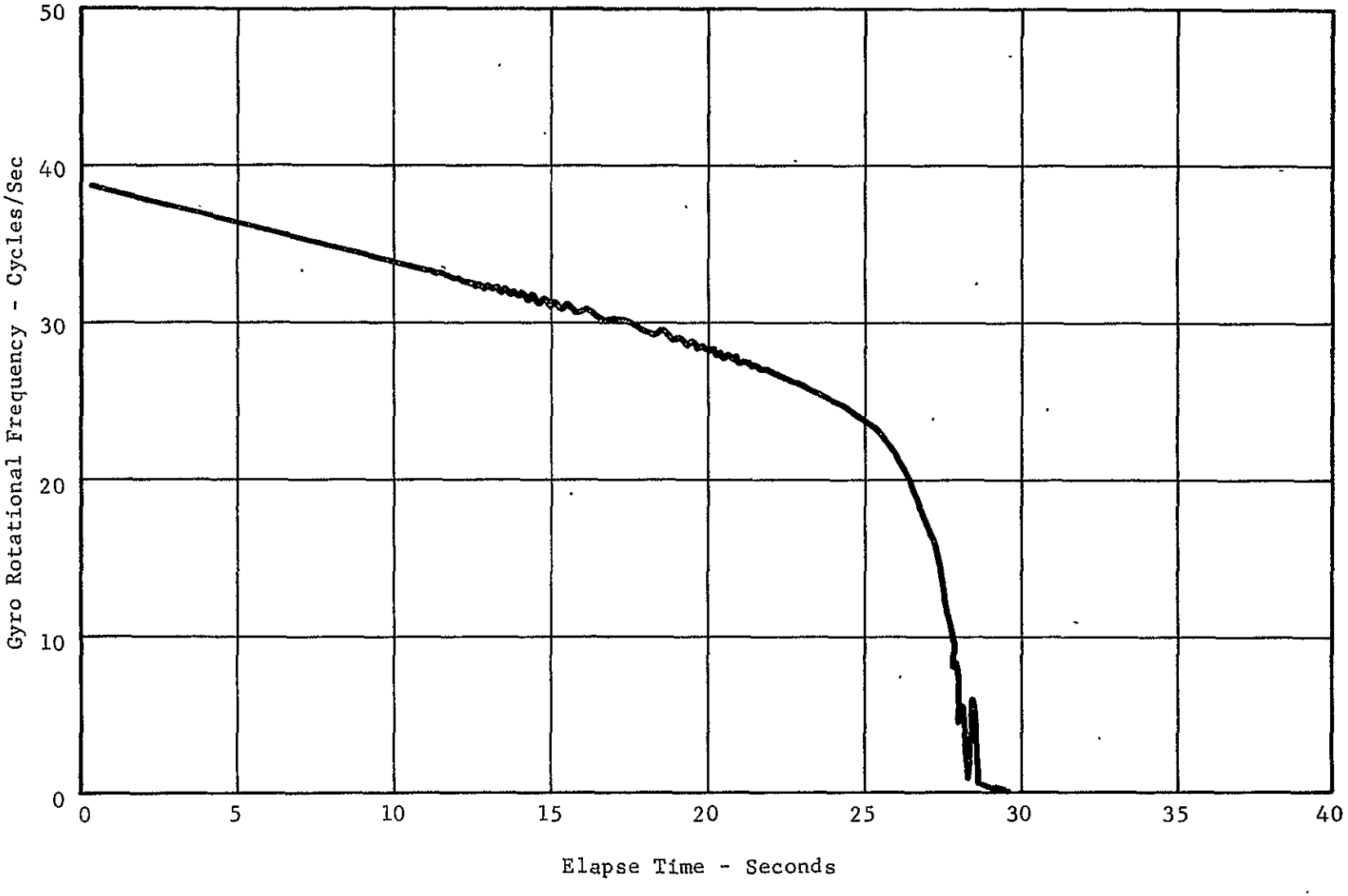

Fig. 9 A Typical Plot of Coast-Down Data from the X-Y Recorder

MTI-7656

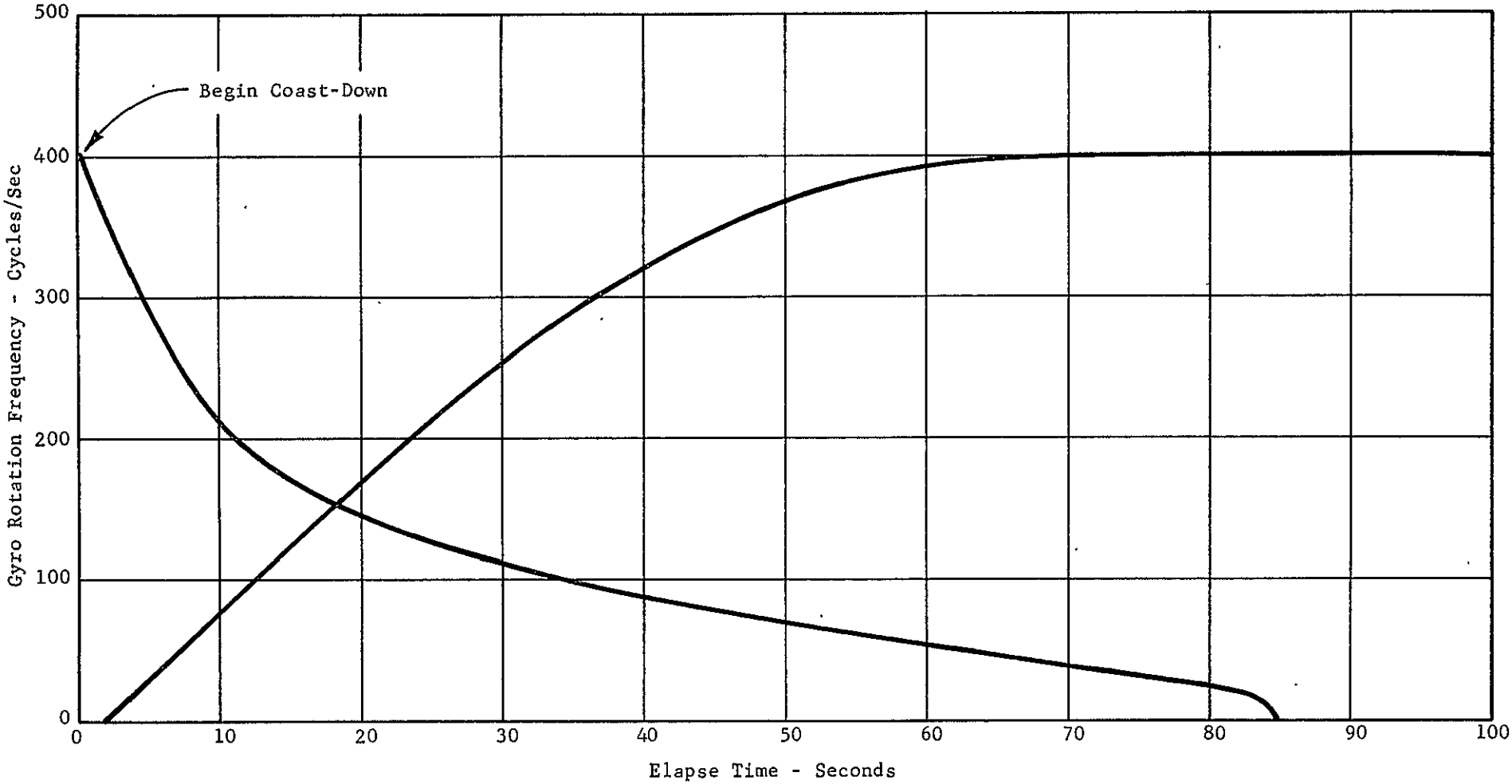

Fig. 10 Start-Up to Synchronous and Coast-Down with the Rotor Axis Horizontal and No Squeeze Film

MTI-7654

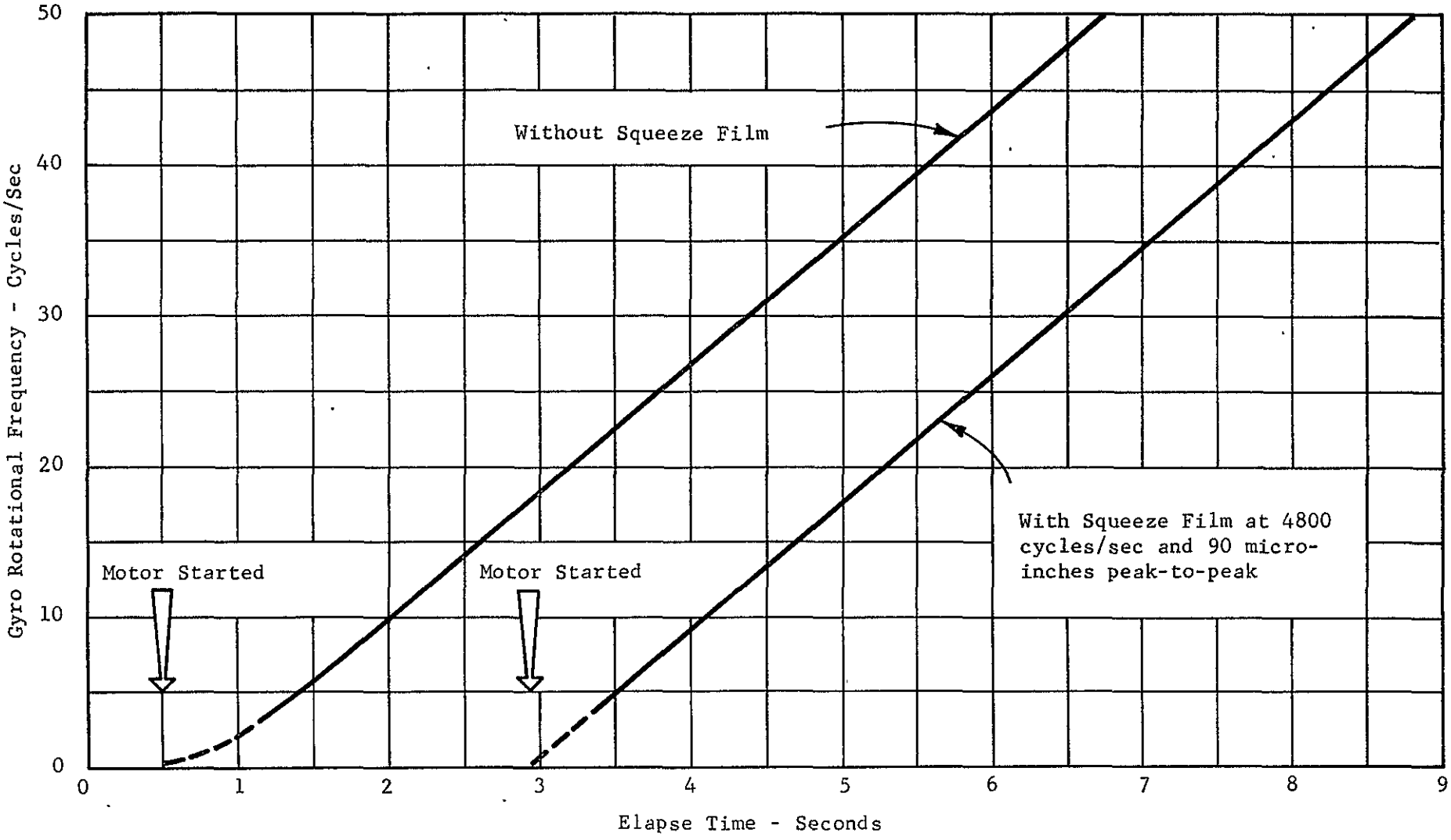

Fig. 11 Two Rotor Start-Ups with Axis Vertical and a Total Axial Bearing Clearance of 110 Microinches

MTI-7660

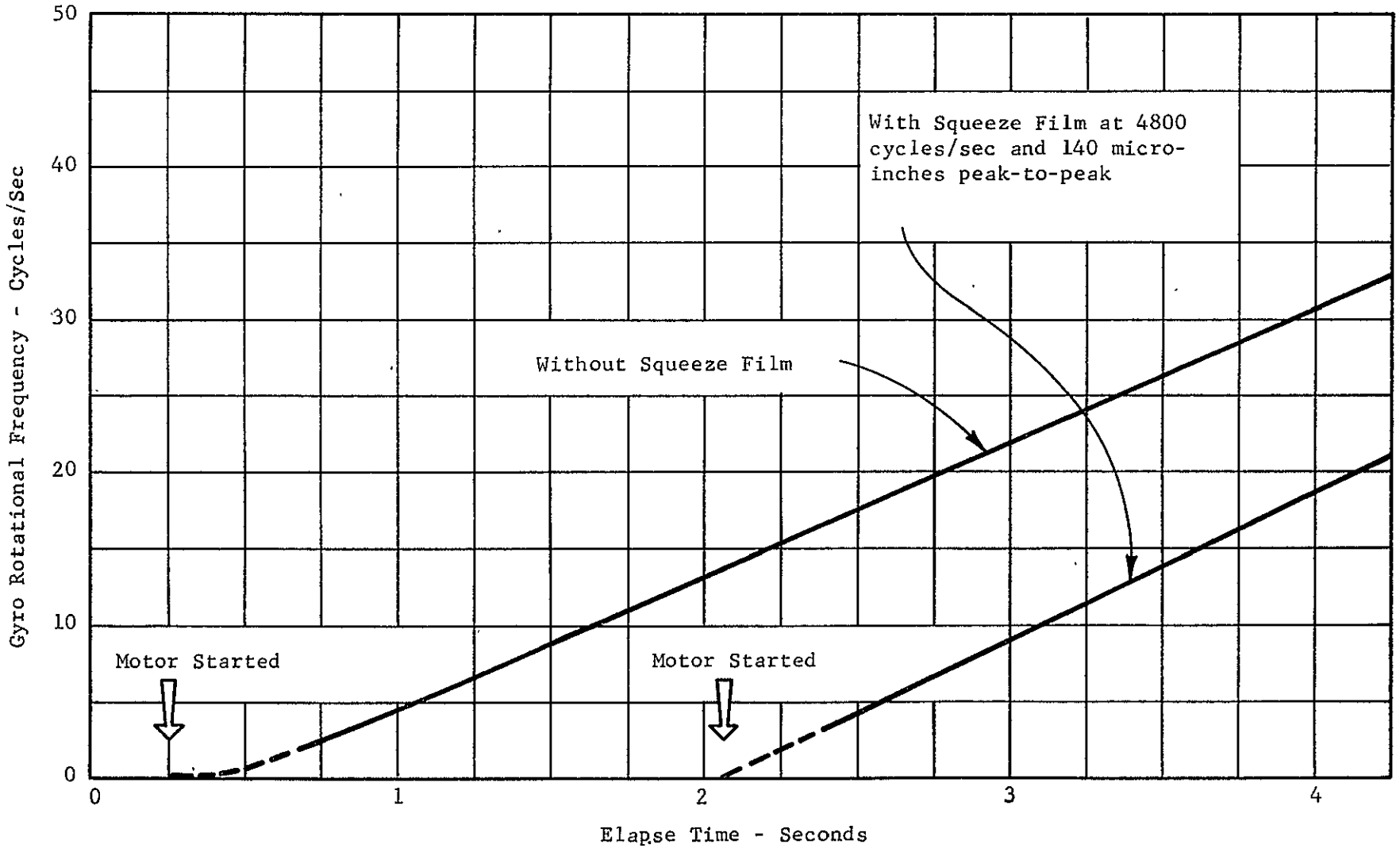

Fig. 12 Two Rotor Start-Ups with Axis Vertical and a Total Axial Bearing Clearance 180 Microinches

MTI-7619

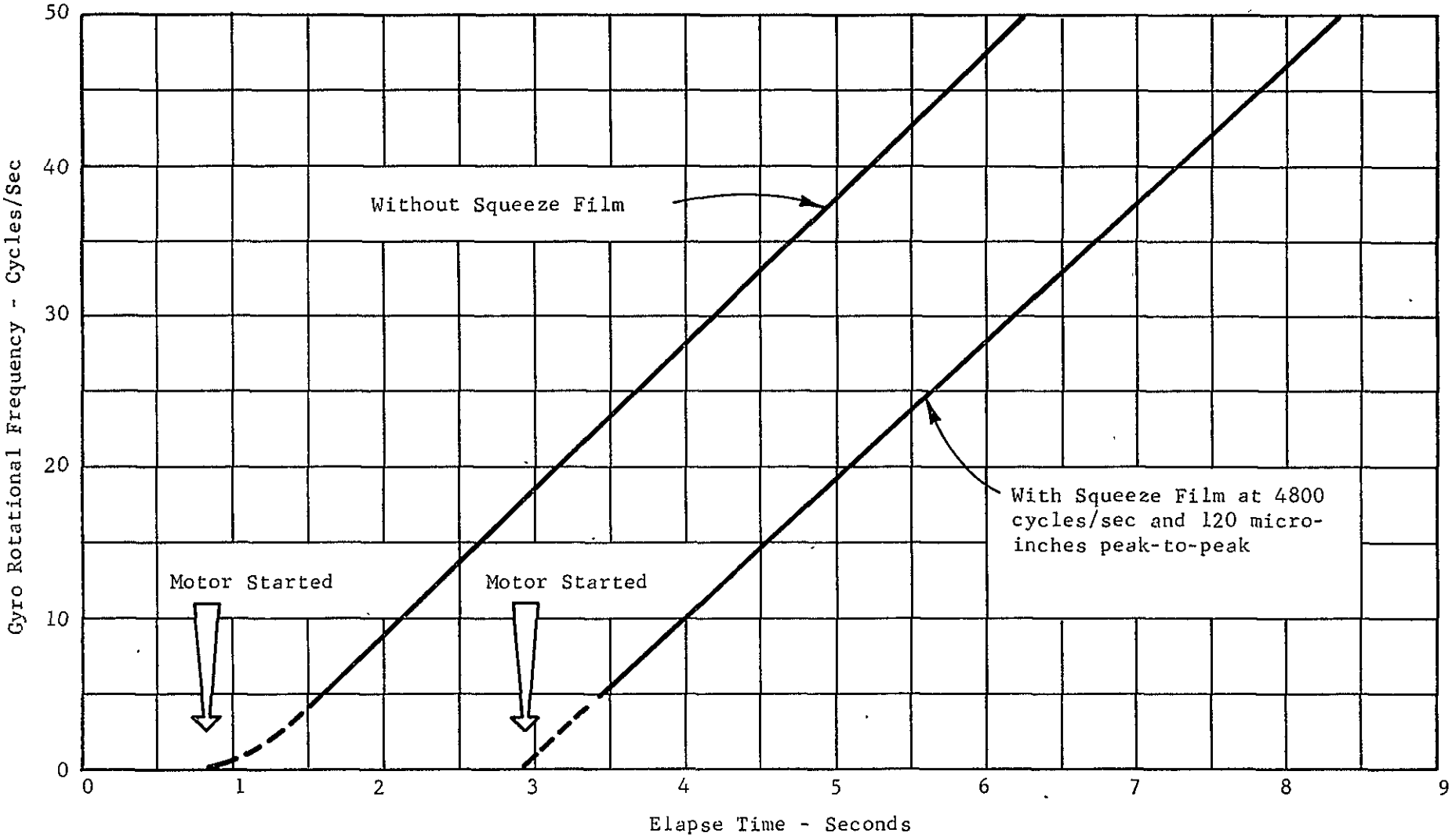

Fig. 13 Two Rotor Start-Ups with Axis Horizontal and a Total Axial Bearing Clearance of 150 Microinches

MTI-7620

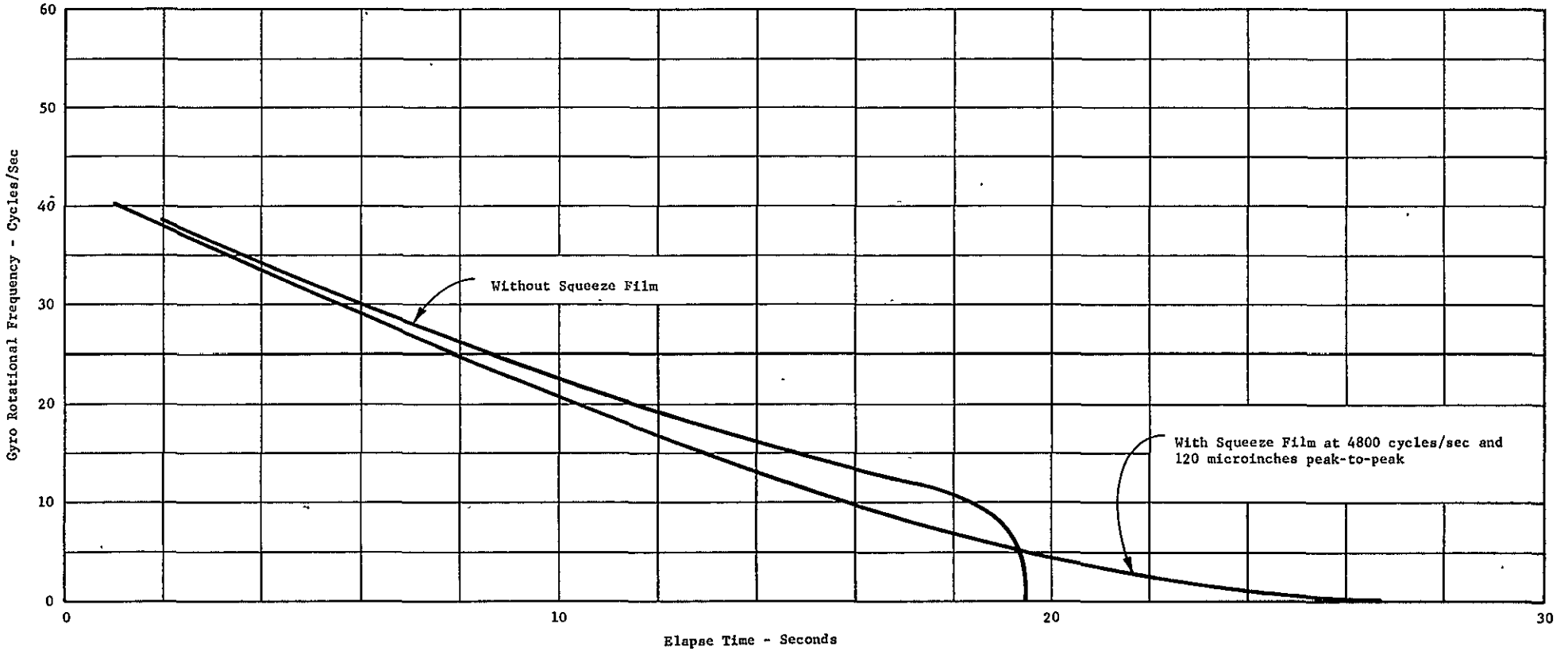

Fig. 14 Coast-Down Curves With the Rotor Axis Horizontal With and Without Squeeze Film at a Total Axial Bearing Clearance of 150 Microinches

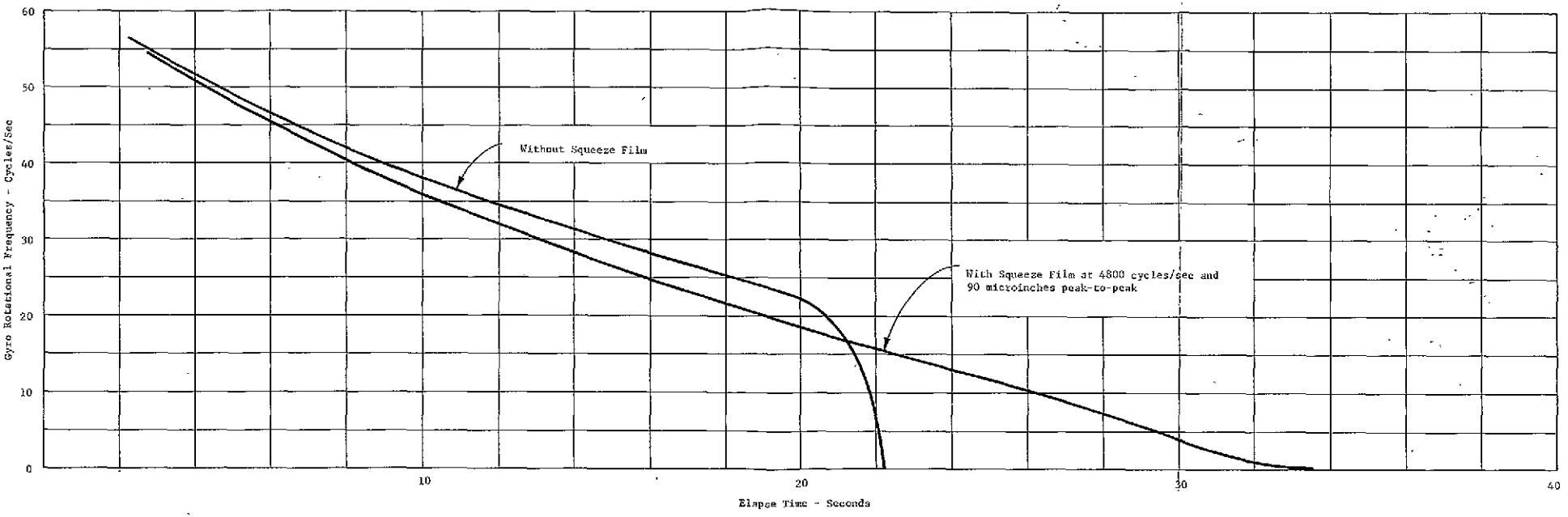

Fig. 15 Coast-Down Curves With and Without Squeeze Film With the Rotor Axis Vertical and a Total Axial Bearing Clearance of 110 Microinches

FOLDOUT FRAME

FOLDOUT FRAME

MIT-7663

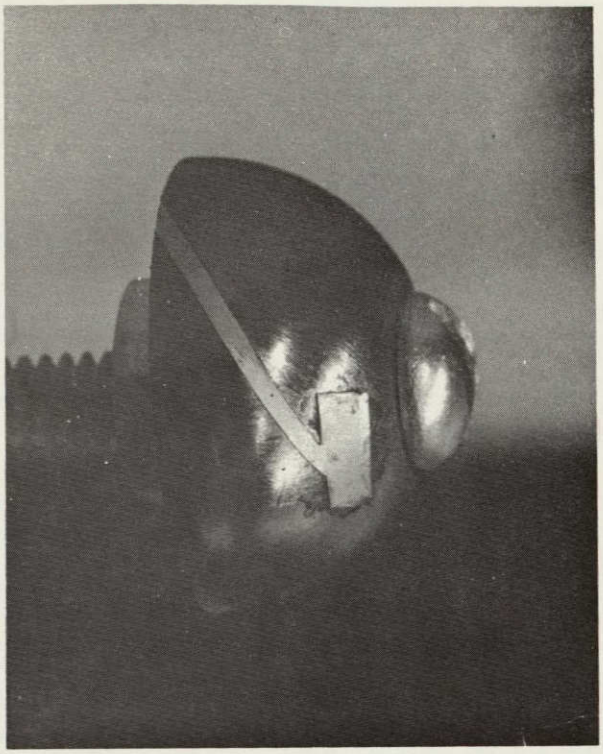

Fig. 17 Male Spherical Bearing with the Brass Land Strip Cemented in Place

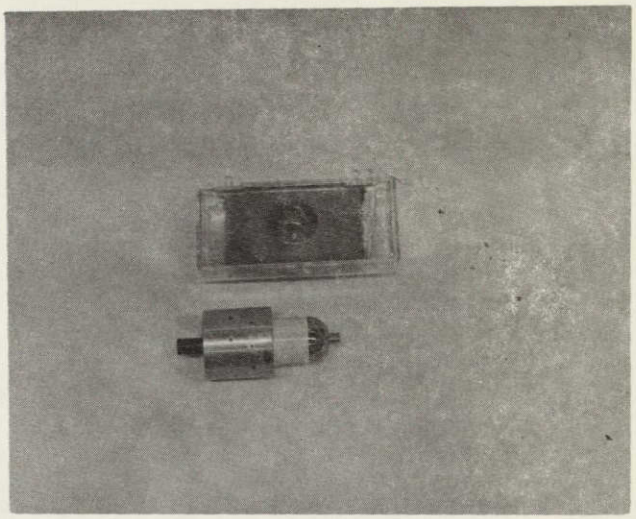

Fig. 18 Male Spherical Bearing on its Holding Fixture and a Conforming Mask on the Metallic Coating with One Land Area Removed

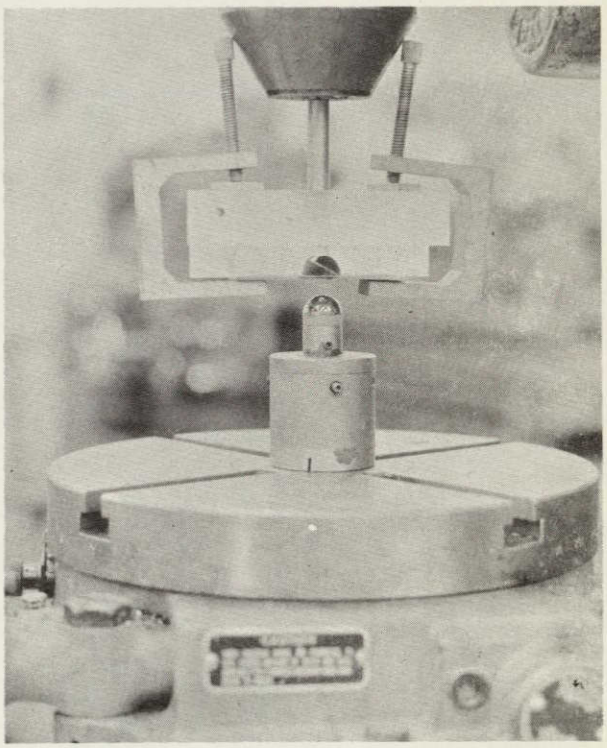

Fig. 19 The Mask is Held in the Spindle of a Milling Machine; One Male Bearing Coated with Photo-resist is Directly Underneath the Mask

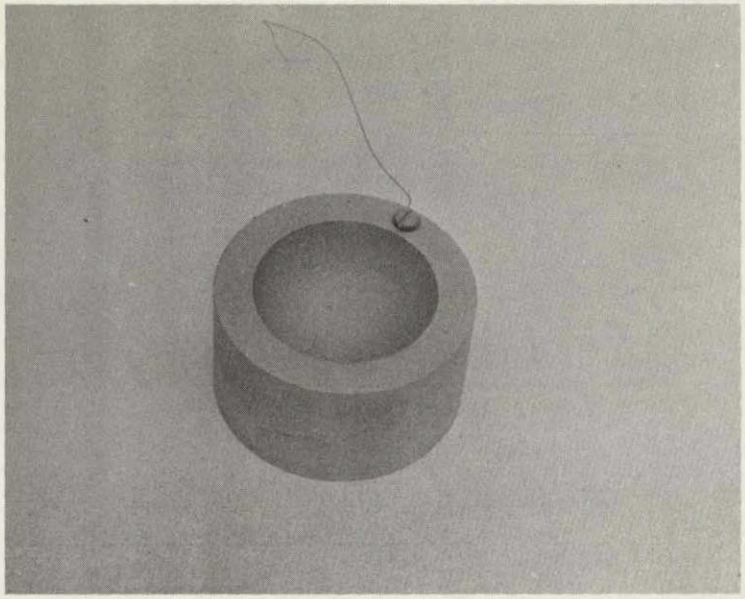

Fig. 20 A Block of 304 Stainless Steel with a Hollow Hemisphere of One Inch Radius

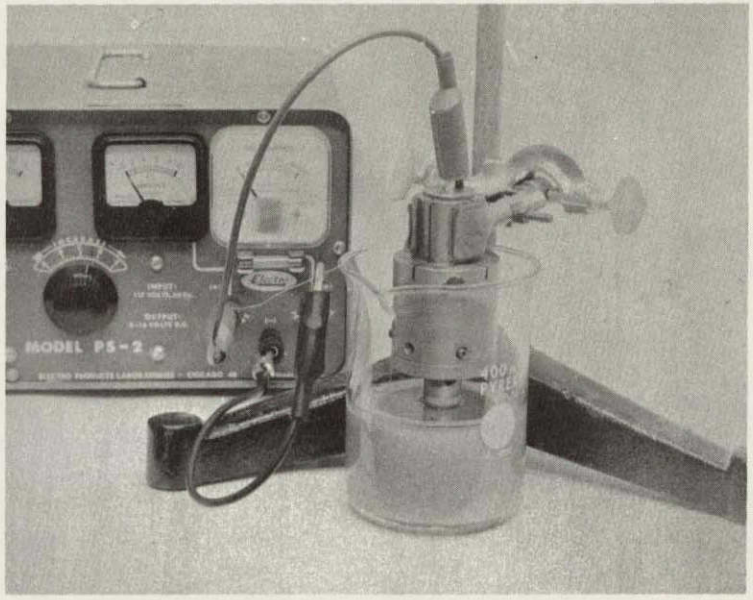

Fig. 21 Etching Pot

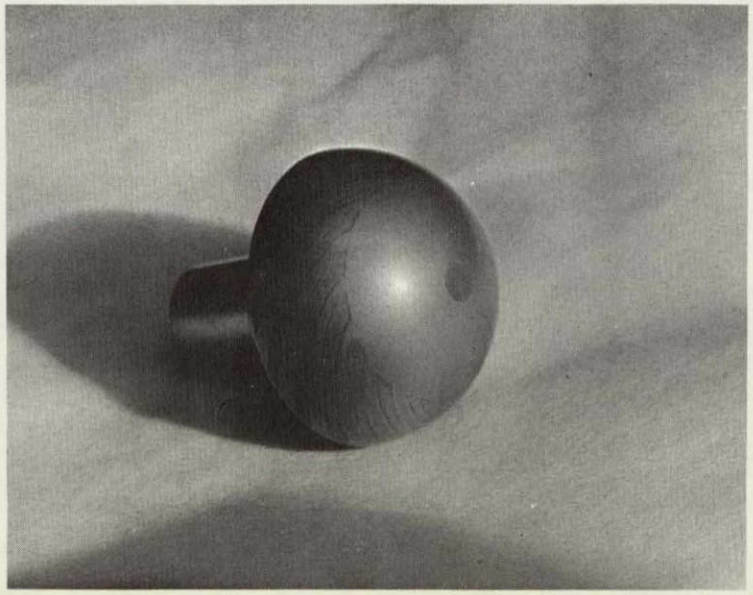

Fig. 22 Etched Spherical Bearing

MTI-7655